Composites Part B 173 (2019) 106815

Contents lists available at ScienceDirect

Composites Part B

journal homepage: www.elsevier.com/locate/compositesb

Boundary layer effect at the edge of fibrous composites using homogenization theory

S. Koley, P.M. Mohite *, C.S. Upadhyay

Department of Aerospace Engineering, Indian Institute of Technology Kanpur, 208016, India

ARTICLE INFO

Keywords:
Composite materials
Micro-structure
Homogenization theory
Boundary layer effect

ABSTRACT

Many studies in the theory of composite materials are based on the homogenization approach, which consists of the substitution of the heterogeneous medium by a homogeneous one with certain effective properties. These effective properties are obtained from internal asymptotics which excludes boundary layer effects. However, at the boundary of the individual ply the periodic solution is disrupted. This loss of periodicity of the interior asymptotic solution needs to be accounted for. Here, the boundary layer solution is a correction in the micro solution which accounts for the applied boundary condition. This error gives rise to a sharp boundary layer which decays very quickly when it travels to the interior of the domain, leaving behind a tail which has to be added to the interior solutions to get the correct representation of the global displacement field. It is shown that this correction is significant, local and affects local stress and strain predictions, which are missed by meso or classical micro mechanical solutions. This important outcome of the study proves the theoretical estimates available in the literature (via error estimates in L^2 and H^1 - norms) emphasizing significant improvement in the local solution at the boundary. It is shown, through numerical examples, that the corrected solution can significantly alter damage initiation predictions at the boundary.

1. Introduction

The homogenization of micro structured composite material is a subject of continuous interest for many years. For this kind of materials, the locally heterogeneous material behaves as a homogeneous media when the characteristic size of the inclusion is much smaller than the size of the whole domain. According to Willis [1] numerous methods in mechanics of composite can be classified into four broad categories: asymptotic, self-consistent, variational, and modeling methods. Most of the methods explained in literature [2,3] accurately predict the effective composite properties provided that the ratio of the RVE size to the global structural dimension is very small, i.e. tending to zero. Well known micro mechanical methods [4,5] include self consistent model [6], concentric cylinder assemblage model [7], method of cells and fully periodic model as shown in Fig. 1. These are the local interior idealization of the micro structure, enabling solution of local problems through which one can predict the effective properties. The solution of this boundary value problem gives the average properties along with the relation between the average and local strains.

Further, local strains can be estimated from the relationship between average and local strains through local structure tensor obtained from the local analysis. The advantage of micromechanical approach is not only to predict the global properties of composites but also to model various micro mechanisms such as damage initiation and propagation. For the analysis, a basic structural element is defined as the smallest element of the microstructure reflecting basic geometrical features. A micrograph of materials, shown in Fig. 2, often displays randomness in distribution thereby making this assumption restrictive.

A brief review presented here deals with the asymptotic approaches explained in literature [8,9] that are capable of analyzing the composite materials with constituents with high distinction in mechanical properties. The asymptotic method for homogenization is detailed in the works by Sanchez-Palencia [10] and Suquet [11]. As remarked by Sanchez-Palencia [10], the two scale asymptotic expansion is a classical method in mechanics. This approach obtains asymptotical developments for the heterogeneous medium in both micro and macro scale. The mathematical theory of homogenization, is used as an alternative approach to find the effective properties of the equivalent homogenized material [12]. The finite element method has been successfully applied in conjunction with the homogenization theory for the analysis of linear

* Corresponding author.
E-mail address: mohite@iitk.ac.in (P.M. Mohite).

https://doi.org/10.1016/j.compositesb.2019.05.026
Received 4 December 2018; Received in revised form 6 March 2019; Accepted 5 May 2019
Available online 12 May 2019

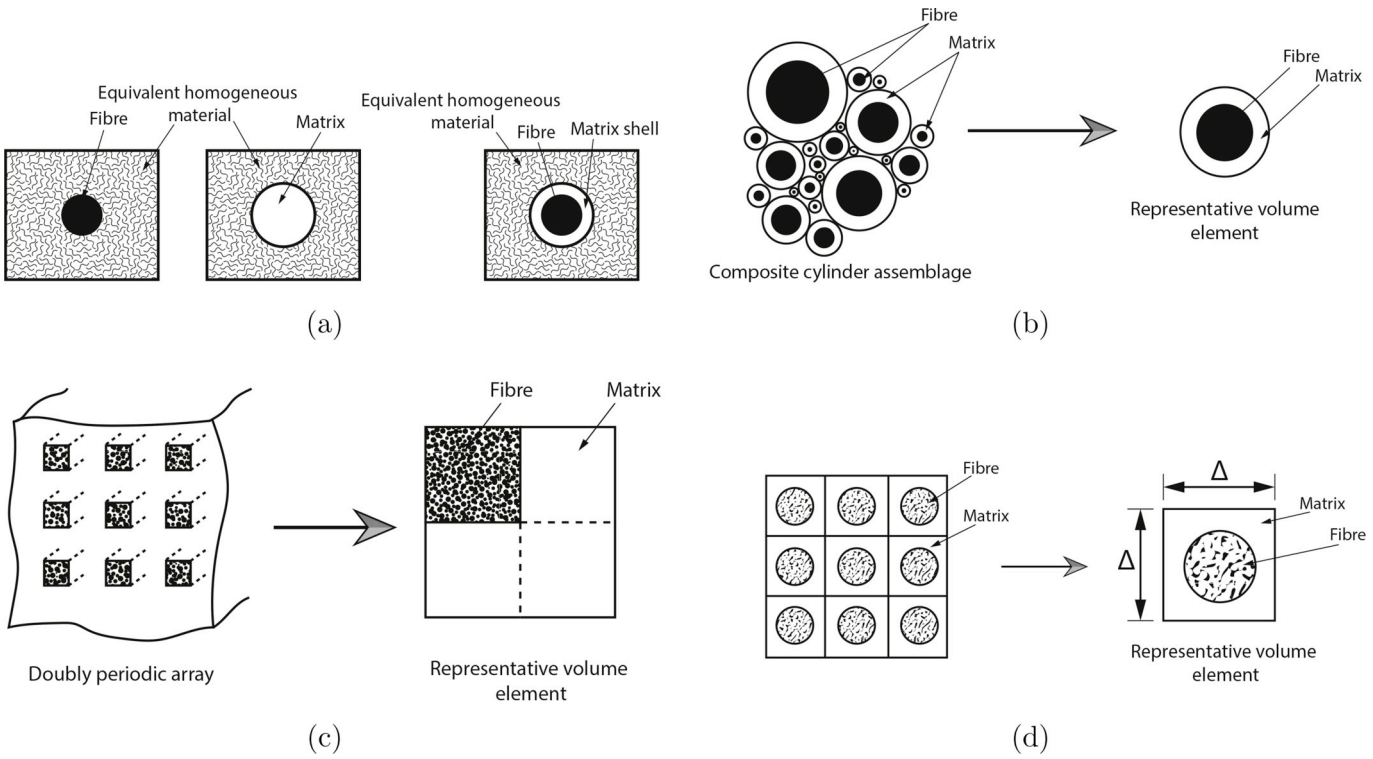

Fig. 1. Different micro mechanical methods for the estimation of the effective properties. (a) Self consistent model and generalized self consistent model, (b) Composite cylinder assemblage (CCA) model, (c) Method of cells, (d) Composite cross section with square periodic arrangement.

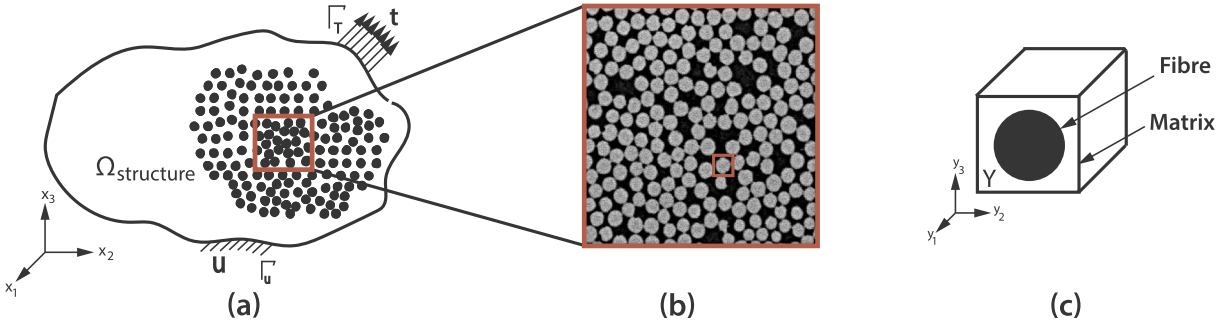

Fig. 2. A heterogeneous system with various levels. (a) A global system, (b) A representative micro structure, (c) A basic unit cell.

elastic fibre reinforced composites by Hollister and Kikuchi [13]. From mathematical point of view the theory of homogenization is a limit theory which uses the asymptotic expansion in Ref. [14] and the assumption of periodicity to substitute the differential equations with rapidly oscillating coefficients. For our problem, we consider the unit cell as shown in Fig. 2 (c). In unit cell models, global properties are determined by assuming macroscopic periodicity conditions on the RVEs. Local problems are solved for specific representative load cases, thus representing the actual interaction between macro and micro scale deformations. Further, novel three dimensional homogenization methods are developed for the design of composites with woven reinforcement [15–18].

It is noteworthy that several authors, e. g, Refs. [19–21] and reference therein, have studied the meso-level boundary layer problem in layered composites. These studies use the effective properties of plies. A number of authors studied the convergence of solutions of equations with rapidly oscillating coefficients to a solution of an averaged equation that does not require the coefficients to be periodic, including a nearly periodic case [22] and sufficient conditions [23] for the convergence of solutions. However, problems relating to the theory of the boundary layer in inhomogeneous media were first treated by Panasenko [24]. Panasenko [25,26] also considered some mathematical questions of the boundary layer theory for inhomogeneous media. However, not much literature is available on the boundary layer tail except the theoretical work done by Allaire and Amar [27], Tartar [28]. Dumontet [29] studied the free edge effects in planar (2D) elastic composite materials with periodic micro structure near a Neumann boundary. The results demonstrate the significance of boundary layer corrections.

In this study, we address the problem of boundary layer in a three-dimensional periodic homogenization for a domain with fixed edges (though the type of boundary condition is not a constraint on the method). Our goal is to investigate how the boundary layer decays from the vicinity of the boundary to the interior of the domain for different fibre orientations. The study is organized as follows: In section 2, the formulation for the asymptotic homogenization for multiple scale analysis starting from the basic elastic continuum is discussed. In section 3, the asymptotic method is extended to the vicinity of the boundary through a boundary layer correction. In section 4 and section 5, numerical implementation and results are discussed, with fibres at different orientations. Plies with 0^0, 45^0 and 90^0 orientations are

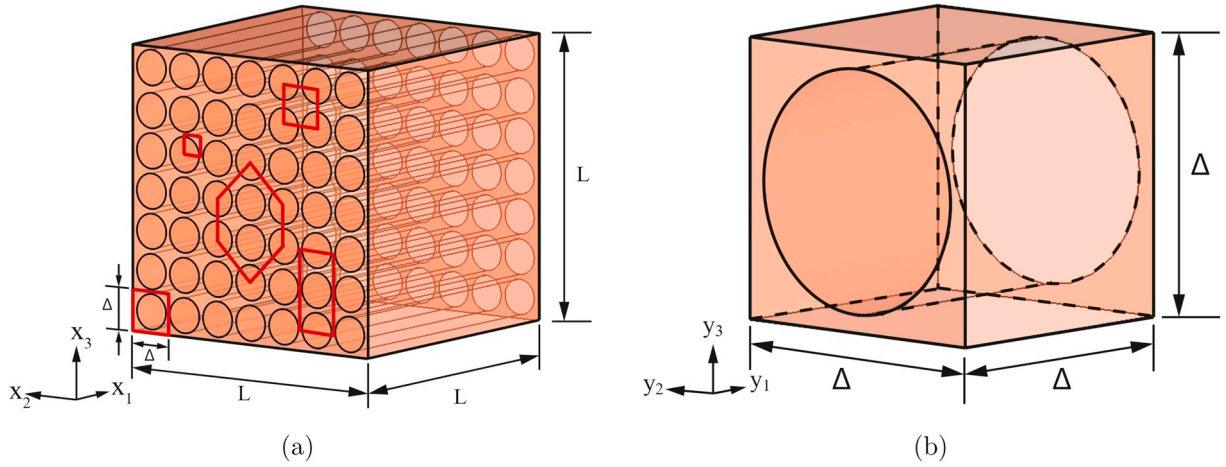

Fig. 3. Macro to micro scale transition. (a) Heterogeneous material at macro scale, (b) Unit cell - RVE for periodic micro structure.

studied. Further the behaviour of the boundary layer for different fundamental load cases is analyzed.

2. Asymptotic homogenization for multiple scale analysis

Homogenization methods have proven to be powerful techniques for the study of heterogeneous media (see Refs. [14,30]). This section describes in detail asymptotic homogenization technique for elasticity [31]. We assume that the material under consideration has a microstructure comprising of two or more different elastic materials which are periodically distributed in all the three directions throughout the material and is represented.

By the unit cell. In the first step, the well known two scale asymptotic expansion method is applied in order to find the precise form of the homogenized equation [31,32]. The existence of two length scales, such as length scale of the microstructure, Δ, and the length scale of the structure, L, is shown in Fig. 3. Different patterns of the unit cell have been shown in Fig. 3 (a), out of which we have taken one pattern (shown in Fig. 3 (b)) as the representative volume element. A numerical finite element method has been employed directly to study the macroscopic behaviour of the structure together with its microstructure. This theory is based on two assumptions: The first one is that the fields vary on multiple scales due to existence of a microstructure and second one is that the microstructure is spatially periodic. The two scales $\boldsymbol{x}$ and $\boldsymbol{y}$ are spatial variables where, $\boldsymbol{x}$ is a macroscopic quantity and $\boldsymbol{y} = \boldsymbol{x}/\Delta$ is a microscopic one as $\boldsymbol{y}$ is associated with the small length scale of the inclusions or heterogeneities.

Considering linear elasticity, where the components of stress tensor σ_{ij} are given as

$$\sigma_{ij} = C_{ijkl}\varepsilon_{kl} \tag{1}$$

using a generalized Hooke's law. The periodic nature of the material is manifested by the scaling relation

$$C^{\Delta}_{ijkl}(\boldsymbol{x}) = C_{ijkl}\left(\frac{\boldsymbol{x}}{\Delta}\right) \tag{2}$$

where, the function C^{Δ}_{ijkl} is $Y-$ periodic in $\boldsymbol{x}$. Let,

$$\varepsilon_{ij}(\boldsymbol{u}^{\Delta}) = \frac{1}{2}\left(\frac{\partial u_i^{\Delta}}{\partial x_j} + \frac{\partial u_j^{\Delta}}{\partial x_i}\right) \tag{3}$$

be the strain field, and

$$\sigma^{\Delta}_{ij} = C^{\Delta}_{ijkl}\varepsilon_{kl}(\boldsymbol{u}^{\Delta}) \tag{4}$$

with, the script Δ denoting quantities that describe the rapidly oscillating behaviour of the material under consideration. Let C^{Δ}_{ijkl} be a periodically oscillating matrix of coefficients. Then the boundary value problem of elasticity is

$$\begin{aligned} &-\frac{\partial}{\partial x_j}\left(C^{\Delta}_{ijkl}\varepsilon_{kl}(\boldsymbol{u}^{\Delta})\right) = f_i \ \text{ in } \ \Omega, \\ &u_i^{\Delta} = 0 \ \text{ on } \ \Gamma_u \ \text{ and } \ \left(C^{\Delta}_{ijkl}\varepsilon_{kl}(\boldsymbol{u}^{\Delta})\right)n_j = t_i \ \text{ on } \ \Gamma_T \end{aligned} \tag{5}$$

which admits a unique solution in $H^1_0 = \left\{\boldsymbol{u}\middle|\frac{1}{2}\int_{\Omega}C^{\Delta}_{ijkl}\varepsilon_{kl}(u^{\Delta})\varepsilon_{ij}(u^{\Delta})dV < \infty, \boldsymbol{u}|_{\Gamma_D} = 0\right\}$. The homogenization of the above equation is a classical issue, which can be seen in the literature (see e.g. Refs. [8,9]). The solution u_i^{Δ} is approximated with an asymptotic series representation in Δ to admit the following ansatz

$$u_i^{\Delta}(\boldsymbol{x}) = u_i^{(0)}(\boldsymbol{x};\boldsymbol{y}) + \Delta\, u_i^{(1)}(\boldsymbol{x};\boldsymbol{y}) + \Delta^2\, u_i^{(2)}(\boldsymbol{x};\boldsymbol{y}) + \ldots + \Delta^n\, u_i^{(n)}(\boldsymbol{x};\boldsymbol{y}) + \ldots \tag{6}$$

where, u_i^{Δ} is the exact value of the field variable, u_i^0 is the macroscopic or average value of the field variable. The displacements $u_i^{(1)}$, $u_i^{(2)}$, …., $u_i^{(m)}$ are the perturbations in the field variable due to the microstructure, also called microstructural displacements. The microstructural displacements $u_i^{(m)}$ are Y - periodic functions with respect to fast variable $\boldsymbol{y}$. The strains $\varepsilon_{ij}(\boldsymbol{u})$ can be expanded as

$$\frac{\partial u_i}{\partial x_j} = \frac{\partial u_i}{\partial x_j} + \frac{\partial u_i}{\partial y_k}\frac{\partial y_k}{\partial x_j} = \frac{\partial u_i}{\partial x_j} + \left(\frac{1}{\Delta}\right)\frac{\partial u_i}{\partial y_j} \tag{7}$$

Substituting Eq. (7) into Eq. (3), we get

$$\varepsilon_{ij}(\boldsymbol{u}^{\Delta}) = \frac{1}{2}\left(\frac{\partial u_i^{\Delta}}{\partial x_j} + \frac{\partial u_j^{\Delta}}{\partial x_i}\right) + \frac{1}{2\Delta}\left(\frac{\partial u_i^{\Delta}}{\partial y_j} + \frac{\partial u_j^{\Delta}}{\partial y_i}\right) \tag{8}$$

The above equation can be further simplified as

$$\frac{1}{2}\left(\frac{\partial u_i^{\Delta}}{\partial x_j} + \frac{\partial u_j^{\Delta}}{\partial x_i}\right) = \overline{\varepsilon}_{ij} \ \text{ and } \ \frac{1}{2}\left(\frac{\partial u_i^{\Delta}}{\partial y_j} + \frac{\partial u_j^{\Delta}}{\partial y_i}\right) = \varepsilon^*_{ij} \tag{9}$$

where, $\overline{\varepsilon}_{ij}$ is the macro, i.e. the smooth part of the strain and ε^*_{ij} is the micro, i.e. the oscillating part which changes rapidly in the periodic medium. The above equation can be expressed in terms of higher powers of Δ as

$$\varepsilon_{ij} = \left(\overline{\varepsilon}_{(0),ij} + \varepsilon^*_{(1),ij}\right) + \Delta\left(\overline{\varepsilon}_{(1),ij} + \varepsilon^*_{(2),ij}\right) + \Delta^2\left(\overline{\varepsilon}_{(2),ij} + \ldots\right) + \ldots \tag{10}$$

with $(\overline{\varepsilon}_{ij} = \sum\Delta^k\, \overline{\varepsilon}_{(k),ij})$ and $(\varepsilon^*_{ij} = \sum\Delta^{k-1}\, \varepsilon^*_{(k),ij})$, which are expressed as

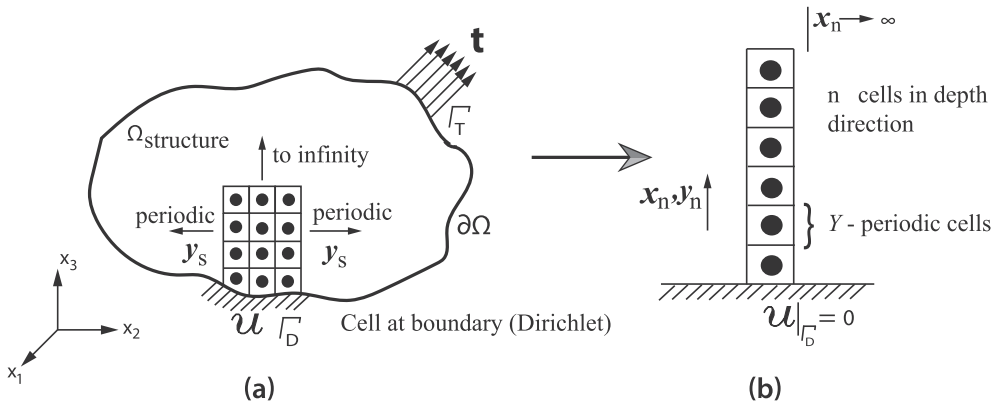

Fig. 4. Elastic body. (a) Elastic body with periodicity only in one direction, (b) y - periodic cells tends to infinity.

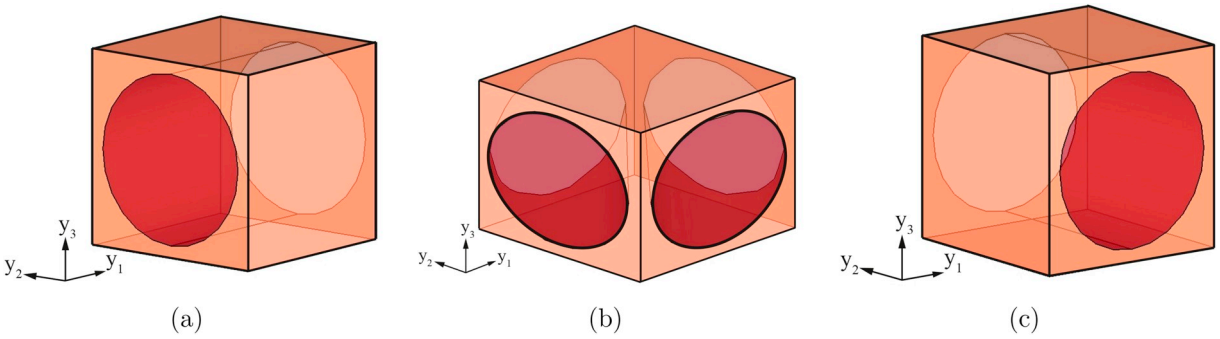

Fig. 5. Unit cell showing different fibre orientations. (a) 0^0, (b) 45^0 and (c).90^0

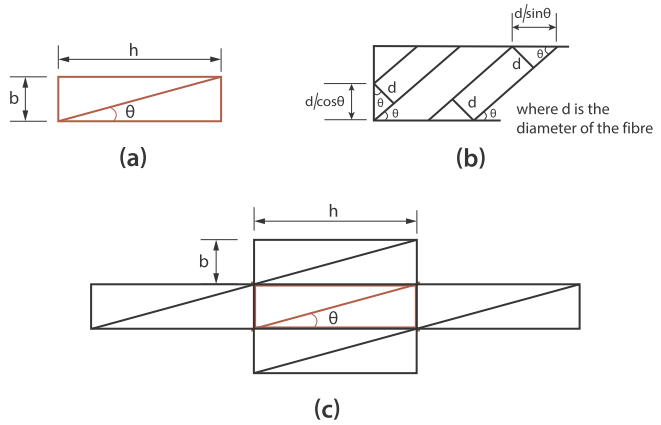

Fig. 6. Unit cell with angular fibre orientation. (a) Unit cell showing the fibre as a line with an angle θ, (b) Size calculation of the RVE for angular fibre orientation, (c) Placing the unit cell on all the sides to check the periodicity of the fibre.

$$\bar{\varepsilon}_{(k),ij}=\frac{1}{2}\left(\frac{\partial u_i^{(k)}}{\partial x_j}+\frac{\partial u_j^{(k)}}{\partial x_i}\right) \text{ and } \varepsilon^*_{(k),ij}=\frac{1}{2}\left(\frac{\partial u_i^{(k)}}{\partial y_j}+\frac{\partial u_j^{(k)}}{\partial y_i}\right) \tag{11}$$

Inserting Eq. (8) using Eq. (9) in Eq. (4), we get

$$\sigma^{\Delta}_{ij}=C^{\Delta}_{ijkl}\bar{\varepsilon}_{kl}+C^{\Delta}_{ijkl}\varepsilon^*_{kl} \tag{12}$$

Further, from Eq. (12), we can write

$$\sigma^{\Delta}_{ij,x_j}=\sigma^{\Delta}_{ij,x_j}+\frac{1}{\Delta}\sigma^{\Delta}_{ij,y_j} \tag{13}$$

$$=\left(C_{ijkl}\bar{\varepsilon}_{kl}\right)_{,x_j}+\left(C_{ijkl}\varepsilon^*_{kl}\right)_{,x_j}+\frac{1}{\Delta}\left(C_{ijkl}\bar{\varepsilon}_{kl}\right)_{,y_j}+\frac{1}{\Delta}\left(C_{ijkl}\varepsilon^*_{kl}\right)_{,y_j}$$

Now, considering the equilibrium equation,

$$\left(C^{(I/M)}_{ijkl}\varepsilon^{(I/M)}_{kl}\right)_{,j}+f_i=0 \tag{14}$$

where, I and M denote inclusion and matrix, respectively. Accounting for powers of Δ, we get the first three expressions as

$$\Delta^{-2}\ :\ \frac{\partial}{\partial y_j}\left[C^{I/M}_{ijkl}\left\{\frac{1}{2}\left(u^{(0)}_{k,y_l}+u^{(0)}_{l,y_k}\right)\right\}\right]=0 \tag{15}$$

$$\Delta^{-1}\ :\ \frac{\partial}{\partial y_j}\left[C^{I/M}_{ijkl}\left\{\frac{1}{2}\left(u^{(0)}_{k,x_l}+u^{(0)}_{l,x_k}+u^{(1)}_{k,y_l}+u^{(1)}_{l,y_k}\right)\right\}\right]$$
$$+\frac{\partial}{\partial x_j}\left[C^{I/M}_{ijkl}\left\{\frac{1}{2}\left(u^{(0)}_{k,y_l}+u^{(0)}_{l,y_k}\right)\right\}\right]=0 \tag{16}$$

$$\Delta^{0}\ :\ \frac{\partial}{\partial x_j}\left[C^{I/M}_{ijkl}\left\{\frac{1}{2}\left(u^{(0)}_{k,x_l}+u^{(0)}_{l,x_k}+u^{(1)}_{k,y_l}+u^{(1)}_{l,y_k}\right)\right\}\right]$$
$$+\frac{\partial}{\partial y_j}\left[C^{I/M}_{ijkl}\left\{\frac{1}{2}\left(u^{(1)}_{k,x_l}+u^{(1)}_{l,x_k}+u^{(2)}_{k,y_l}+u^{(2)}_{l,y_k}\right)\right\}\right]+f_i=0 \tag{17}$$

Due to the consistency requirement (see Eq. (15) - Eq. (16)) the multipliers of Δ^{-2} and Δ^{-1} should become zero, leading to

$$u^{(0)}_k(\boldsymbol{x}) \text{ is independent of } \boldsymbol{y}$$
$$\frac{\partial}{\partial y_j}\left(C_{ijkl}\bar{\varepsilon}_{(0),kl}+C_{ijkl}\varepsilon^*_{(1),kl}\right)=0 \tag{18}$$

Expressing,

$$\varepsilon^*_{(1),kl}=\tilde{\varepsilon}^{mn}_{kl}\bar{\varepsilon}_{(0),mn} \tag{19}$$

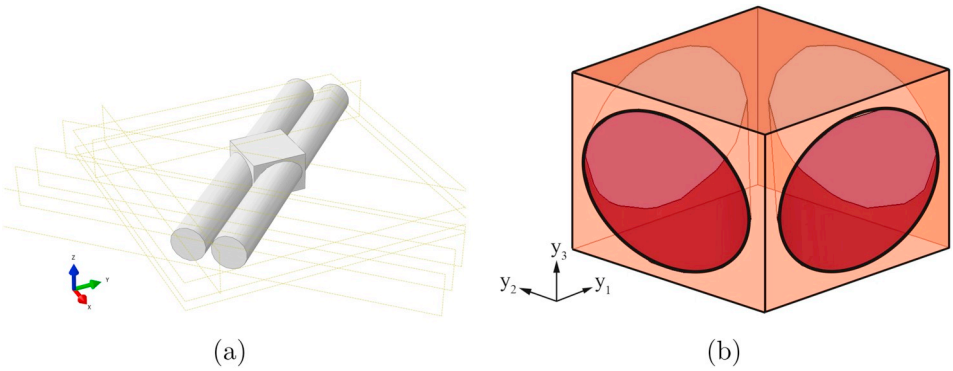

Fig. 7. Unit cell. (a) Modeling fibres with angular orientation, (b) Unit cell with angular fibre orientation.

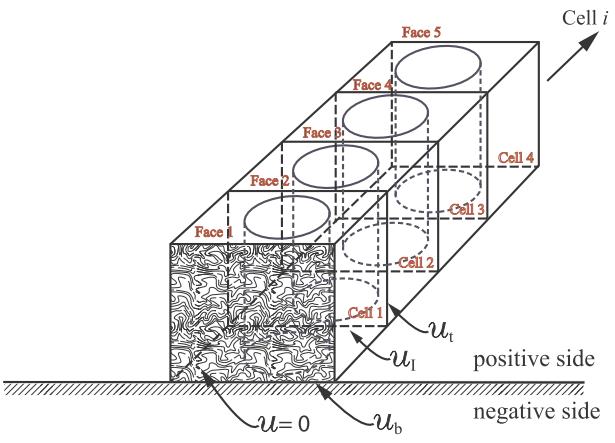

Fig. 8. Unit cell in the vicinity of the boundary towards the interior of the domain (showing the displacement boundary condition).

the second of Eq. (18) can be rewritten as,

$$\left[\frac{\partial}{\partial y_j}\left(C_{ijkl}+C_{ijmn}\,\tilde{\varepsilon}^{kl}_{mn}\right)\right]\overline{\varepsilon}_{(0),kl}=0 \tag{20}$$

where, the above equation is a purely Y - domain problem. The above condition is true for any value of $\overline{\varepsilon}_{(0),kl}$. Note that the above representation requires the solution of six fundamental problems corresponding to each $\overline{\varepsilon}_{(0),ij}$, the solution of which can be given as $\chi^{(ij)}$, with $\chi^{(ij)}$ a fully periodic function in the Y - domain (or unit cell). Thus,

$$\tilde{\varepsilon}^{(kl)}_{mn}=\frac{1}{2}\left(\chi^{(kl)}_{m,y_n}+\chi^{(kl)}_{n,y_m}\right) \tag{21}$$

The six periodic fundamental solutions corresponding to $\overline{\varepsilon}_{(0),mn}$ can be solved using Eq. (20). From the equilibrium Eq. (17) and the consistency condition, we get

$$\int_{V_{RVE}}\left[C_{ijkl}\left(\delta_{km}\delta_{ln}+\tilde{\varepsilon}^{mn}_{kl}\right)\left(\overline{\varepsilon}_{(0),mn}\right)_{,x_j}+f_i\right]dV=0 \tag{22}$$

Finally, dividing by the volume of the RVE, we get

$$\frac{1}{V_{RVE}}\left[\int_{V_{RVE}}\left\{C_{ijkl}\left(\delta_{km}\delta_{ln}+\tilde{\varepsilon}^{mn}_{kl}\right)dV\right\}\right]\left(\overline{\varepsilon}_{(0),mn}\right)_{,x_j}+f_i=0 \tag{23}$$

Further, from this expression we have

$$\frac{1}{V_{RVE}}\left[\int_{V_{RVE}}\left\{C_{ijkl}\left(\delta_{km}\delta_{ln}+\tilde{\varepsilon}^{mn}_{kl}\right)dV\right\}\right]=\overline{C}_{ijmn} \tag{24}$$

which is the RVE volume averaged (or effective) global stiffness used for ply-level macro solutions. The homogenized tensor $\overline{C}_{ijkl}$ may be

Table 1
Mechanical properties of AS4 carbon fibre material by Soden et al. [35].

E_1 (GPa)	E_2 (GPa)	G_{12} (GPa)	G_{23} (GPa)	ν_{12}
225	15	15	7	0.2

Table 2
Mechanical properties of 3501-6 epoxy matrix material by Soden et al. [35].

E (GPa)	G (GPa)	ν
4.2	1.567	0.35

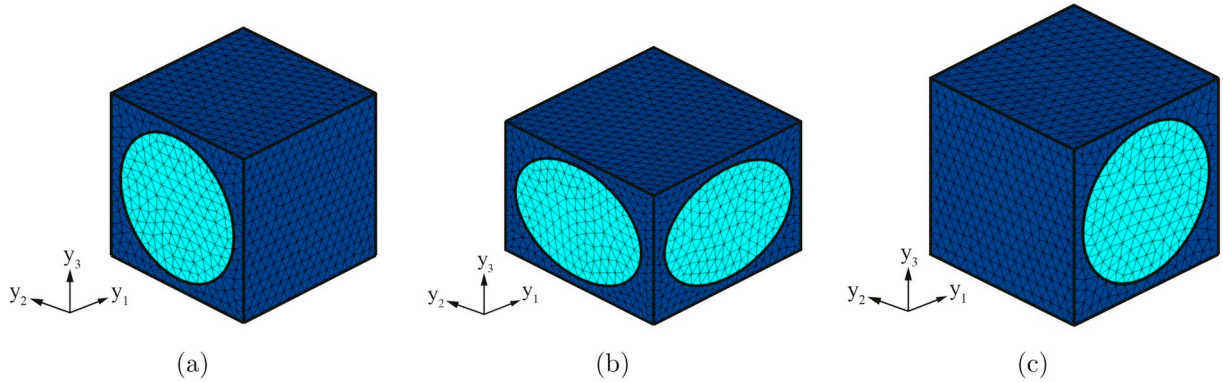

Fig. 9. Finite element model of RVEs with different fibre orientations. (a) 0^0 fibre orientation, (b) 45^0 fibre orientation, (c) 90^0 degree fibre orientation.

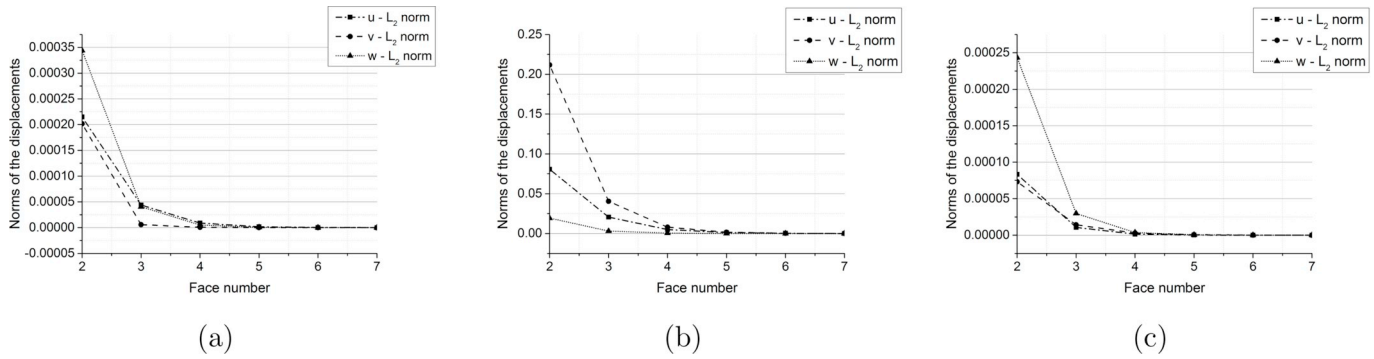

Fig. 10. Decay of the minimum displacement norms for different fibre orientations from Face 2 to Face 7 (a) 0° - ($\varepsilon_{(0),xx}$), (b) 45° - ($\varepsilon_{(0),yy}$) and (c) 90° - ($\varepsilon_{(0),xx}$).

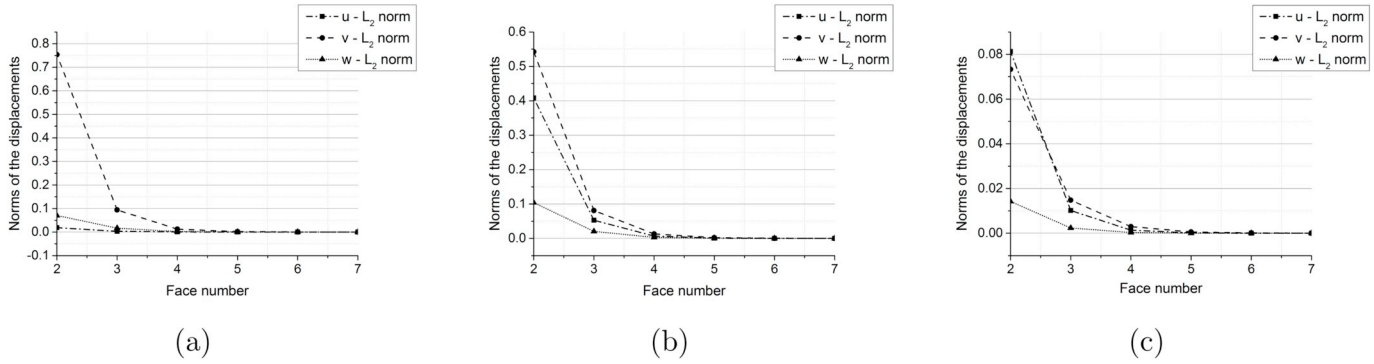

Fig. 11. Decay of the maximum displacement norms for different fibre orientations from Face 2 to Face 7 (a) 0° - ($\varepsilon_{(0),yz}$), (b) 45° - ($\varepsilon_{(0),yz}$) and (c) 90° - ($\varepsilon_{(0),yz}$).

Table 3
Extreme values of the displacement norm for different fibre orientation.

Orientation	0°		45°		90°	
MIN/MAX Value	MIN	MAX	MIN	MAX	MIN	MAX
Macro Strain	$\varepsilon_{(0),xx}$	$\varepsilon_{(0),yz}$	$\varepsilon_{(0),yy}$	$\varepsilon_{(0),yz}$	$\varepsilon_{(0),xx}$	$\varepsilon_{(0),yz}$
Norm Value	$2.07E-09$	$7.54E-01$	$3.8E-06$	$5.42E-01$	$2.94E-09$	$8.13E-02$
Displacement Norm	$\|\|v\|\|_{L_2}$	$\|\|v\|\|_{L_2}$	$\|\|w\|\|_{L_2}$	$\|\|v\|\|_{L_2}$	$\|\|u\|\|_{L_2}$	$\|\|u\|\|_{L_2}$
Layers to Decay	4–5	6–7	4–5	5–6	4–5	5–6

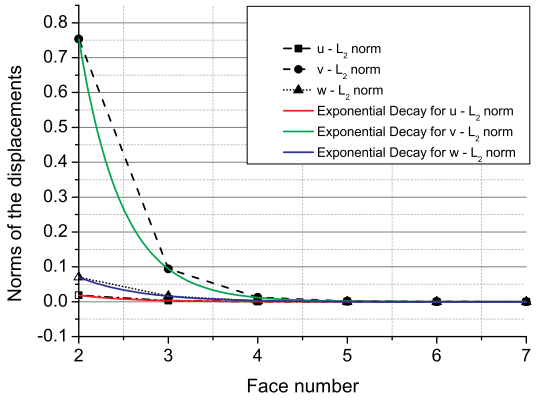

		Value for $\varepsilon_{(0),yz}$
u - L_2 norm	A	0.70881
	t	0.55074
v - L_2 norm	A	48.47479
	t	0.48030
w - L_2 norm	A	1.32084
	t	0.68425

(b)

Fig. 12. Exponential decay of the maximum displacement norm for 0° fibre orientation. (a) Macro strain ($\varepsilon_{(0),yz}$), (b) Decay constants for u, v and w - L_2 norm.

interpreted as a physical parameter corresponding to an effective macro-level homogeneous material, where overall response is 'close' to that of the heterogeneous material, when the size of the cell tends to zero.

Theorem 2.1. *Following the work in* [27], *let* $\boldsymbol{u}^{\Delta}$ *be the unique solution of the exact boundary value problem given by Eq. (5), then the approximation* $\tilde{\boldsymbol{u}}(\boldsymbol{x},\boldsymbol{y}) \approx \boldsymbol{u}_0(\boldsymbol{x}) + \Delta\boldsymbol{u}_1(\boldsymbol{x};\boldsymbol{y})$ *converges weakly to* $\boldsymbol{u}^{\Delta}$ *in* $H_0^1(\Omega)$ *as*:

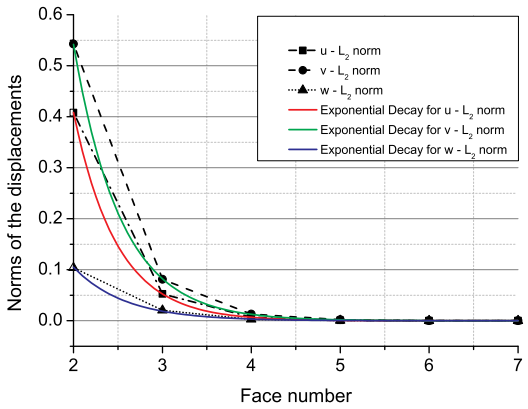

(a)

		Value for $\varepsilon_{(0),yz}$
u - L_2 norm	A	24.60250
	t	0.48796
v - L_2 norm	A	23.44199
	t	0.53084
w - L_2 norm	A	3.28057
	t	0.58104

(b)

Fig. 13. Exponential decay of the maximum displacement norm for 45° fibre orientation. (a) Macro strain ($\varepsilon_{(0),yz}$), (b) Decay constants for u, v and w - L_2 norm.

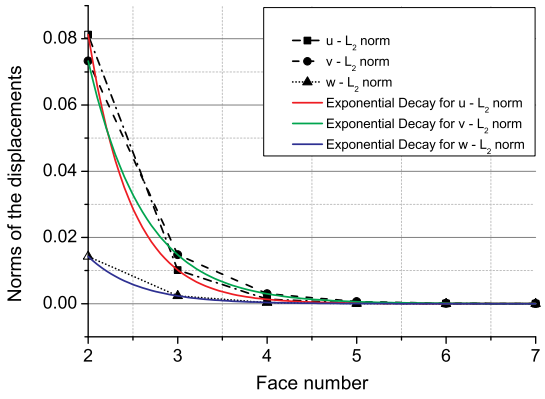

(a)

		Value for $\varepsilon_{(0),yz}$
u - L_2 norm	A	5.20083
	t	0.48084
v - L_2 norm	A	1.80435
	t	0.62430
w - L_2 norm	A	0.51689
	t	0.55710

Fig. 14. Exponential decay of the maximum displacement norm for 90° fibre orientation. (a) Macro strain ($\varepsilon_{(0),yz}$), (b) Decay constants for u, v and w - L_2 norm.

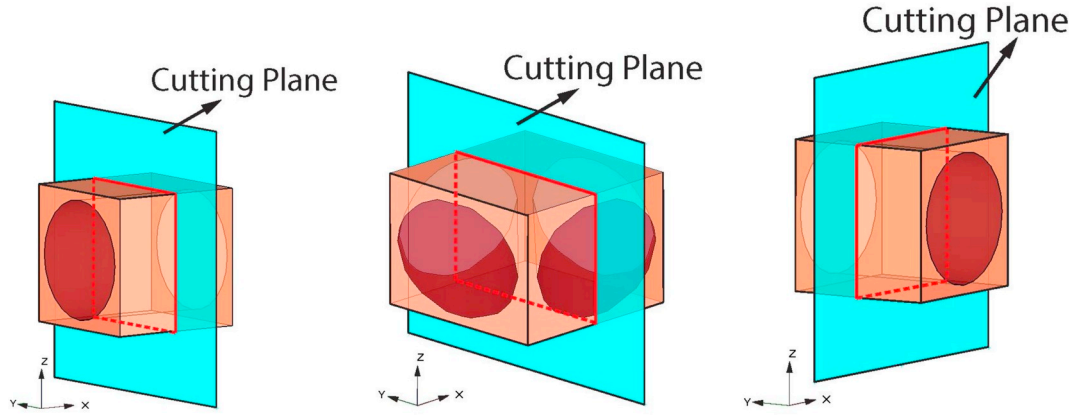

(a) (b) (c)

Fig. 15. RVEs showing cutting plane. (a) 0^0 fibre orientation, (b) 45^0 fibre orientation, (c) 90^0 fibre orientation.

$$\left|\left|\boldsymbol{u}^{\Delta}(\boldsymbol{x}) - \tilde{\boldsymbol{u}}(\boldsymbol{x};\boldsymbol{y})\right|\right|_{H^1(\Omega)} \leq C\sqrt{\Delta} \tag{25}$$

where the expression in Eq. (25) is for the fully periodic problem and $\boldsymbol{u}_1$ is given by

$$\boldsymbol{u}_1(\boldsymbol{x};\boldsymbol{y}) = \sum_{m,n=1}^{3} \boldsymbol{\chi}^{mn}(\boldsymbol{y})\bar{e}_{(0),mn} + \overline{\boldsymbol{u}}(\boldsymbol{x}) \tag{26}$$

3. Problems in the vicinity of the boundary

Due to the boundary layer phenomenon, the homogenized system depends in a non trivial way on the boundary. Consider the cell at the boundary of the composite material, as shown in Fig. 4, with homogeneous Dirichlet boundary condition, $\boldsymbol{u}^{(\Delta)}(\boldsymbol{x};\boldsymbol{y}) = 0$ on Γ_D. We expect the solution $\boldsymbol{u}^{\Delta}$ as

Table 4
Extreme values of micro strains for applied normal macro strain for both boundary layer (BL) and fully periodic (FP) problems for RVE with 0° fibre orientation.

Macro Strain		$\varepsilon_{(0),xx}$		$\varepsilon_{(0),yy}$		$\varepsilon_{(0),zz}$	
		BL	FP	BL	FP	BL	FP
|Strain Value|	MIN	0.0014	0.00046	0.026	0.022	0.036	0.017
	MAX	0.013	0.012	0.390	1.200	0.940	1.100
Strain Type	MIN	$\varepsilon^{(bl)}_{,xx}$	$\varepsilon_{(1),xx}$	$\varepsilon^{(bl)}_{xx}$	$\varepsilon_{(1),xx}$	$\varepsilon^{(bl)}_{xx}$	$\varepsilon_{(1),xx}$
	MAX	$\varepsilon^{(bl)}_{xy}$	$\varepsilon_{(1),zz}$	$\varepsilon^{(bl)}_{xy}$	$\varepsilon_{(1),yy}$	$\varepsilon^{(bl)}_{yz}$	$\varepsilon_{(1),zz}$

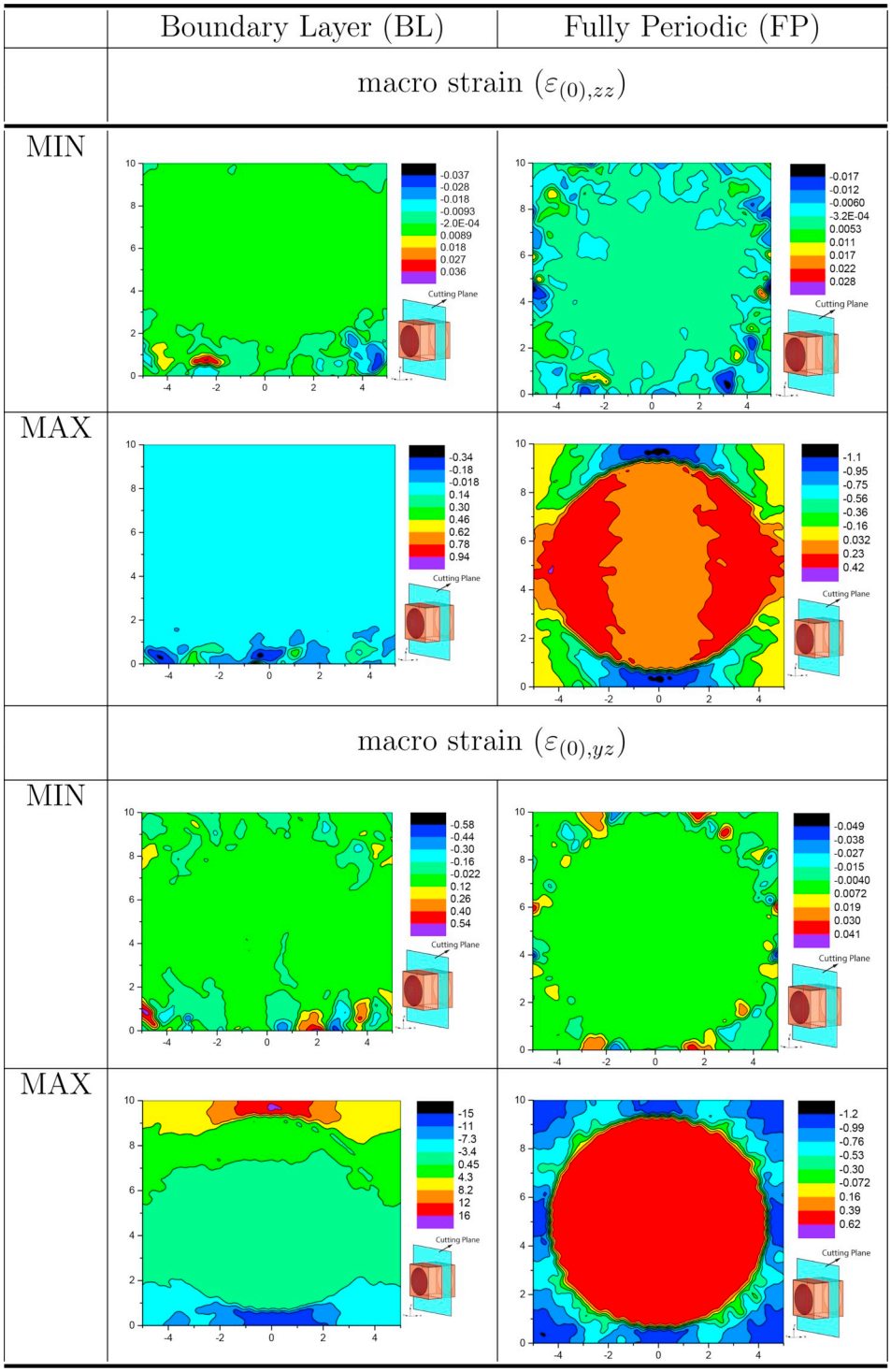

Fig. 16. Comparison of micro strain for BL and FP problem - normal and shear load cases for 0° RVE.

Table 5
Extreme values of micro strains for applied shear macro strain for both boundary layer (BL) and fully periodic (FP) problems for RVE with 0° fibre orientation.

Macro Strain		$\varepsilon_{(0),yz}$		$\varepsilon_{(0),xz}$		$\varepsilon_{(0),xy}$	
		BL	FP	BL	FP	BL	FP
|Strain Value|	MIN	0.540	0.041	0.160	0.051	0.190	0.048
	MAX	16	1.200	4.400	4	4	3.900
Strain Type	MIN	$\varepsilon_{yy}^{(bl)}$	$\varepsilon_{(1),xx}$	$\varepsilon_{xx}^{(bl)}$	$\varepsilon_{(1),zz}$	$\varepsilon_{yy}^{(bl)}$	$\varepsilon_{(1),yy}$
	MAX	$\varepsilon_{xz}^{(bl)}$	$\varepsilon_{(1),yz}$	$\varepsilon_{yz}^{(bl)}$	$\varepsilon_{(1),xz}$	$\varepsilon_{xz}^{(bl)}$	$\varepsilon_{(1),xy}$

$$u_i^{\Delta}(\boldsymbol{x};\boldsymbol{y}) = u_i^{(0)}(\boldsymbol{x}) + \Delta\, u_i^{(1)}(\boldsymbol{x};\boldsymbol{y}) + \text{ h.o.t.} \tag{27}$$

The above expression works well for the internal asymptotics, i.e. for the periodic solution. However, we need to enforce $u_i^{\Delta}(\boldsymbol{x};\boldsymbol{y}) = 0$, at the boundary. Since $u_i^{(0)}(\boldsymbol{x}) = 0$ is enforced on the boundary but $u_i^{(1)}(\boldsymbol{x};\boldsymbol{y})$ is not necessarily zero at the boundary, there is a violation of displacement boundary condition and the hypothesis of Y - periodicity is not true in the vicinity of the boundary. Thus,

$$\boldsymbol{u}^{(0)}|_{\Gamma} + \Delta\boldsymbol{u}^{(1)}|_{\Gamma} = \boldsymbol{u}|_{\Gamma_D} = 0 \text{ is desired but } \boldsymbol{u}^{(1)}|_{\Gamma} \neq 0 \tag{28}$$

Hence, we need a correction in this term, i.e. a function that is negative of $u_i^{(1)}(\boldsymbol{x};\boldsymbol{y})$ at boundary and decays to zero as we move far away from the vicinity of the boundary. This forms a displacement field due to a boundary layer, i.e. $u_i^{(bl)}(\boldsymbol{x};\boldsymbol{y})$. Here, the superscript '*bl*' stands for boundary layer. To improve the asymptotic expansion near the boundary, we need to introduce additional terms, called boundary layer [27,33,34]. Thus, Eq. (27) becomes

$$u_i^{\Delta}(\boldsymbol{x};\boldsymbol{y}) = u_i^{(0)}(\boldsymbol{x}) + \Delta\left(u_i^{(1)}(\boldsymbol{x};\boldsymbol{y}) + u_i^{(bl)}(\boldsymbol{x};\boldsymbol{y})\right) + \text{ h.o.t.} \tag{29}$$

The advantage of ansatz of Eq. (29) over Eq. (6) is that each term $(u_i^{(1)} + u_i^{(bl)})$ satisfies a Dirichlet boundary condition. Note that $u_i^{(bl)}(\boldsymbol{x};\boldsymbol{y})$ depends on $\boldsymbol{y}$, but is not a periodic function with respect to the second argument.

The boundary layer term $\boldsymbol{u}^{(bl)}$ is equivalently defined by

$$\boldsymbol{u}^{(bl)}(\boldsymbol{x};\boldsymbol{y}) = \boldsymbol{\chi}^{(bl),mn}(\boldsymbol{x};\boldsymbol{y})\varepsilon_{(0),mn}(\boldsymbol{x}) \tag{30}$$

with

$$\boldsymbol{u}^{(bl)}(\boldsymbol{x};\boldsymbol{y})|_{\Gamma_D} = -\boldsymbol{u}_{(1)}(\boldsymbol{x};\boldsymbol{y})|_{\Gamma_D} \tag{31}$$

and

$$\boldsymbol{u}^{(bl)}(\boldsymbol{x}\to\infty;\boldsymbol{y}) = \boldsymbol{c}(\boldsymbol{x}) \tag{32}$$

Further,

$$\chi_i^{(bl),mn}(\boldsymbol{x};\boldsymbol{y}_s + \boldsymbol{y}_p) = \chi_i^{(bl),mn}(\boldsymbol{x};\boldsymbol{y}_s) \tag{33}$$

which means there is tangential periodicity along the boundary plane with a period $\boldsymbol{y}_p$ and there is no periodicity along the depth direction $(\boldsymbol{x}_n,\boldsymbol{y}_n)$. With such a boundary layer correction, the convergence result of Theorem 2.1 can be improved and is expressed in the next section. For this boundary layer problem, the strain can be expressed as

$$\varepsilon_{ij} \approx \left(\overline{\varepsilon}_{(0),ij} + \varepsilon^*_{(1),ij} + \varepsilon^{*(bl)}_{ij}\right) + \Delta\left(\overline{\varepsilon}_{(1),ij} + \overline{\varepsilon}^{(bl)}_{ij}\right) \tag{34}$$

Substituting the above equation in the equilibrium condition and collecting terms, we get

$$\begin{aligned}&\frac{\partial}{\partial x_j}\left[C_{ijkl}\left(\overline{\varepsilon}_{(0),kl} + \varepsilon^*_{(1),kl} + \varepsilon^{*(bl)}_{kl}\right) + \Delta\left(\overline{\varepsilon}_{(1),kl} + \overline{\varepsilon}^{(bl)}_{kl}\right)\right] + f_i \\ &+\frac{1}{\Delta}\frac{\partial}{\partial y_j}\left[C_{ijkl}\left(\overline{\varepsilon}_{(0),kl} + \varepsilon^*_{(1),kl} + \varepsilon^{*(bl)}_{kl}\right)\right] + \Delta\left[C_{ijkl}\left(\overline{\varepsilon}_{(1),kl} + \overline{\varepsilon}^{(bl)}_{kl}\right)\right] = 0\end{aligned} \tag{35}$$

Again, for $\Delta\to 0$, using the consistency condition, we get $\boldsymbol{u}^{(0)}(\boldsymbol{x})$ as a function of $\boldsymbol{x}$ only and for the Δ^{-1} term we get

$$\frac{\partial}{\partial y_i}\left\{C_{ijkl}\left(\overline{\varepsilon}_{(0),kl} + \varepsilon^*_{(1),kl} + \varepsilon^{*(bl)}_{kl}\right)\right\} = 0 \tag{36}$$

Using the interior asymptotic construction given earlier, we get

$$\frac{\partial}{\partial y_i}\left\{C_{ijkl}\left(\overline{\varepsilon}_{(0),kl} + \varepsilon^*_{(1),kl}\right)\right\} = 0 \text{ and } \frac{\partial}{\partial y_i}\left(C_{ijkl}\varepsilon^{*(bl)}_{kl}\right) = 0 \tag{37}$$

In the above equation the term $\varepsilon^{*(bl)}_{kl}$ is due to the boundary layer, which is solved using a periodic column, as shown in Fig. 4 (b). The first expression of Eq. (37) is for the fully periodic problem and the second expression is for the boundary layer problem, respectively. The second expression in Eq. (37) shows that the boundary layer problem does not have a driving force, but is only driven by the mismatch in the boundary condition given by Eq. (36) which can be rewritten as:

$$\frac{\partial}{\partial y_j}\left(C_{ijkl}\widehat{\varepsilon}^{mn}_{kl}\right)\varepsilon_{(0),mn} = 0 \tag{38}$$

where,

$$\widehat{\varepsilon}^{mn}_{kl} = \frac{1}{2}\left(\frac{\partial\chi_k^{(bl),mn}}{\partial y_l} + \frac{\partial\chi_l^{(bl),mn}}{\partial y_k}\right) \tag{39}$$

The above condition means that.

(1) u_i^{bl} is not required to be fully Y - periodic,
(2) u_i^{bl} is taken to be y_s - periodic as the mismatch along boundary Γ_D is periodic (this means that we need to solve u_i^{bl} for only one column of cells starting from Γ_D) and
(3) We want $u_i^{bl}(\boldsymbol{x}\to\infty;\boldsymbol{y})\to c_i$, a constant.

Theorem 3.1. *Following the work in* [27], *let* $\boldsymbol{u}^{\Delta}$ *be the unique solution to* Eq. (5) *then,*

$$\left|\left|\boldsymbol{u}^{\Delta}(\boldsymbol{x}) - \boldsymbol{u}^{(0)}(\boldsymbol{x}) - \Delta\boldsymbol{u}^{(1)}(\boldsymbol{x};\boldsymbol{y}) - \Delta\boldsymbol{u}^{(bl)}(\boldsymbol{x};\boldsymbol{y})\right|\right|_{H^1_0(\Omega)} \leq C\Delta \tag{40}$$

Furthermore, for any open set (ω) embedded in Ω there exists a constant C_1, independent of Δ such that,

$$\left|\left|\boldsymbol{u}^{\Delta}(\boldsymbol{x}) - \boldsymbol{u}^{(0)}(\boldsymbol{x}) - \Delta\boldsymbol{u}^{(1)}(\boldsymbol{x};\boldsymbol{y}) - \Delta\boldsymbol{u}^{(bl)}(\boldsymbol{x};\boldsymbol{y})\right|\right|_{L^2(\omega)} \leq C_1\Delta^{\frac{3}{2}} \tag{41}$$

From the above expression we can justify that,

Table 6
Extreme values of micro strains for applied normal macro strain for both boundary layer (BL) and fully periodic (FP) problems for RVE with 90° fibre orientation.

Macro Strain		$\varepsilon_{(0),xx}$		$\varepsilon_{(0),yy}$		$\varepsilon_{(0),zz}$	
		BL	FP	BL	FP	BL	FP
|Strain Value|	MIN	0.00147	0.00765	0.0475	0.0176	0.0238	0.018
	MAX	0.0143	0.0625	0.4860	4.2400	1.0200	4.360
Strain Type	MIN	$\varepsilon_{xx}^{(bl)}$	$\varepsilon_{(1),xx}$	$\varepsilon_{xx}^{(bl)}$	$\varepsilon_{(1),xx}$	$\varepsilon_{xx}^{(bl)}$	$\varepsilon_{(1),xx}$
	MAX	$\varepsilon_{yy}^{(bl)}$	$\varepsilon_{(1),yz}$	$\varepsilon_{xz}^{(bl)}$	$\varepsilon_{(1),yz}$	$\varepsilon_{xy}^{(bl)}$	$\varepsilon_{(1),yz}$

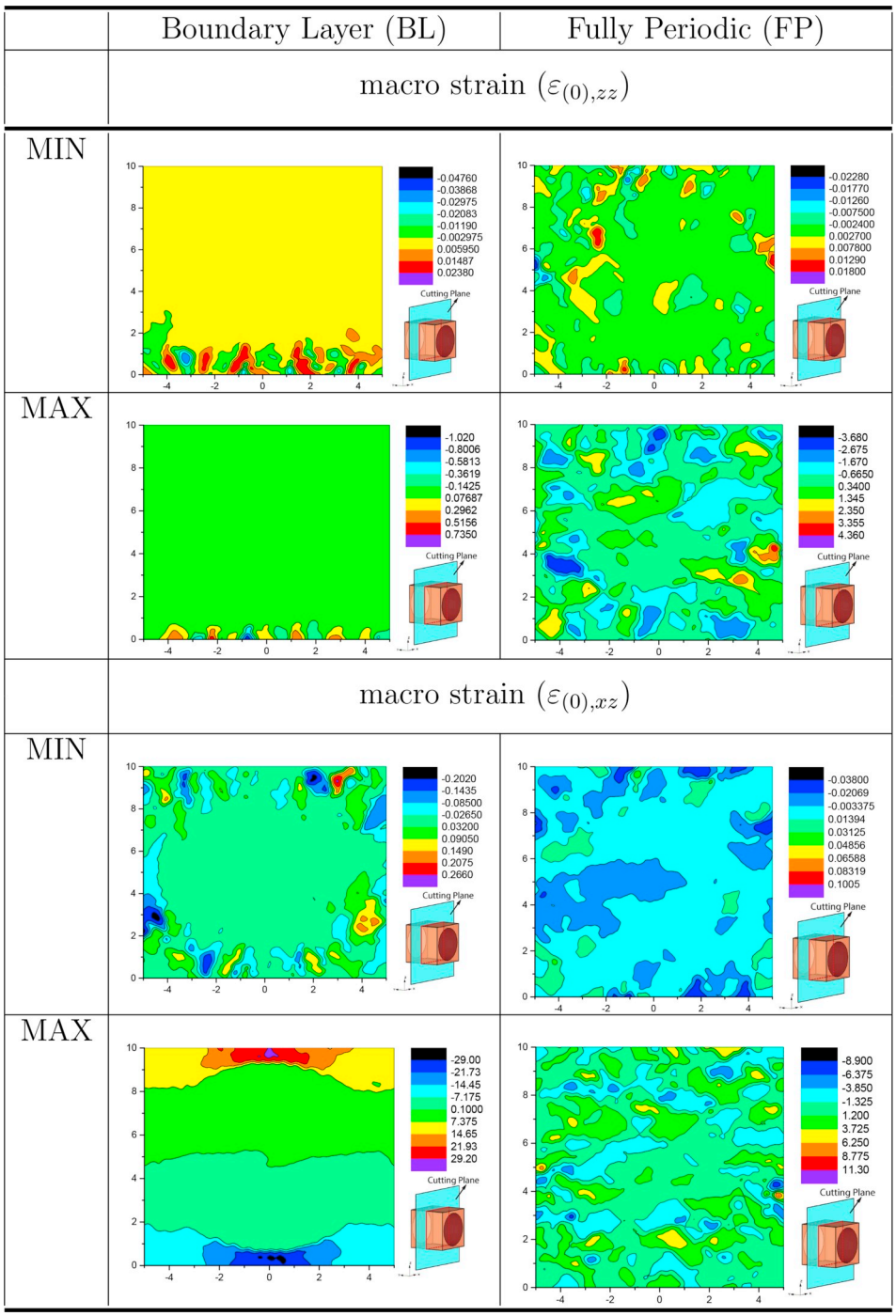

Fig. 17. Comparison of micro strain for BL and FP problem - normal and shear load cases for 90° RVE.

Table 7
Extreme values of micro strains for applied shear macro strain for both boundary layer (BL) and fully periodic (FP) problems for RVE with 90° fibre orientation.

Macro Strain		$\varepsilon_{(0),yz}$		$\varepsilon_{(0),xz}$		$\varepsilon_{(0),xy}$	
		BL	FP	BL	FP	BL	FP
|Strain Value|	MIN	0.220	0.026	0.202	0.038	0.206	0.0384
	MAX	4.500	8	29.200	11.300	3.100	8.500
Strain type	MIN	$\varepsilon_{yy}^{(bl)}$	$\varepsilon_{(1),xx}$	$\varepsilon_{xx}^{(bl)}$	$\varepsilon_{(1),yy}$	$\varepsilon_{yy}^{(bl)}$	$\varepsilon_{(1),zz}$
	MAX	$\varepsilon_{xz}^{(bl)}$	$\varepsilon_{(1),yz}$	$\varepsilon_{yz}^{(bl)}$	$\varepsilon_{(1),xz}$	$\varepsilon_{xy}^{(bl)}$	$\varepsilon_{(1),xy}$

Table 8
Extreme values of micro strains for applied normal macro strain for both boundary layer (BL) and fully periodic (FP) problems for RVE with 45° fibre orientation.

Macro Strain		$\varepsilon_{(0),xx}$		$\varepsilon_{(0),yy}$		$\varepsilon_{(0),zz}$	
		BL	FP	BL	FP	BL	FP
|Strain Value|	MIN	0.210	0.112	0.153	0.117	0.127	0.123
	MAX	2.680	2.430	3.200	2.550	2.180	1.130
Strain Type	MIN	$\varepsilon_{zz}^{(bl)}$	$\varepsilon_{(1),zz}$	$\varepsilon_{zz}^{(bl)}$	$\varepsilon_{(1),zz}$	$\varepsilon_{zz}^{(bl)}$	$\varepsilon_{(1),yy}$
	MAX	$\varepsilon_{xy}^{(bl)}$	$\varepsilon_{(1),xx}$	$\varepsilon_{xy}^{(bl)}$	$\varepsilon_{(1),yy}$	$\varepsilon_{xy}^{(bl)}$	$\varepsilon_{(1),zz}$

$$\boldsymbol{u}_{recons}^{(bl)} = \boldsymbol{u}^{(0)} + \Delta\boldsymbol{u}^{(1)} + \boldsymbol{u}^{(bl)} \tag{42}$$

So, the error $\boldsymbol{e}^{(bl)}$ is given as

$$\boldsymbol{e}^{(bl)} = \boldsymbol{u}_{ex} - \boldsymbol{u}_{recons}^{(bl)} \tag{43}$$

where, $\boldsymbol{u}_{recons}^{(bl)}$ denotes the reconstructed boundary layer solution, $\boldsymbol{u}^{(1)}$ is the displacement for the fully periodic problem and $\boldsymbol{u}_{ex}$ is the exact displacement.

Theorem 3.1 indicates that the boundary layer correction leads to an optimal convergence rate for the error (as a function of Δ) in the H_0^1 - norm. However, in the L_2 - norm the rate is better than the classical result (i.e. $\Delta^{\frac{3}{2}}$ instead of Δ) but is still non-optimal. Note that the two-dimensional result of Dumontet [29] shows a significant improvement in the solution due to boundary-layer correction. In the following sections, we will carry out a detailed study of the three-dimensional influence of boundary, for the specific case of Dirichlet boundary.

4. Basic concept of generation of RVE

As in most micromechanical analysis of composite materials, regular packing has been assumed, typically in a square or hexagonal layout as shown in Fig. 3. A micromechanical model is set up based on periodic RVE technique for continuous reinforced composite. It is assumed that fibres are uniformly distributed in a matrix and have the same radii as shown in Fig. 3 (b).

Therefore, each unidirectional layer can be represented by a unit cube with a single fibre having the required fibre volume fraction. Here, three different scenarios are considered as unit cell with fibre in three directions as 0^0, 45^0 and 90^0 and are shown in Fig. 5. When modeling the unit cell with fibre orientation 45^0, periodicity has to be enforced carefully. For angle-ply, a specific strategy has been followed by which initially a rectangle of height b and width h is considered and then a line segment is placed diagonally as a fibre as shown in Fig. 6 (a). This rectangle is the master unit cell.

Now, this master unit cell is placed on all the four sides as shown in Fig. 6 (c), and a check is done to ascertain whether the fibres are running continuously, maintaining the periodicity on all the sides with the same angle as that of the master unit cell. Now the diagonal line is replaced by a fibre of diameter d, with the master unit cell defined by height, $h = \frac{d}{cos\theta}$ and width, $b = \frac{d}{sin\theta}$. Now considering this as a base, three dimensional RVE is modeled to create the periodic unit cell. For this we assume a rational number and from Fig. 6 (a) it can be said that,

$$tan\theta = \left(\frac{b}{h}\right) = (\text{any rational number}) \tag{44}$$

For example, if $tan\theta = \frac{1}{3}$, then $\left(\frac{b}{h} = \frac{1}{3}\right)$, $3b = h$, i.e. the unit cell should have a width that is three times the height. This will also ensure the periodicity of the angular fibre on both faces of the unit cell. As an example, an RVE is modeled with fiber orientation 45^0 with fibre volume fraction of 0.6 (see Fig. 7). The periodic column at the boundary is constructed, as shown in Fig. 8, by stacking unit periodic cells.

5. Numerical formulation of the problem

The linear system of equations resulting from the finite element analysis of the boundary layer problem given by Eq. (38) is of the form

$$\boldsymbol{K}\boldsymbol{u} = \boldsymbol{f} \tag{45}$$

$\boldsymbol{K}$ is symmetric and semi-positive definite, while the right side vector $\boldsymbol{f}$ denotes the nodal forces due to the boundary conditions. Now, considering a single unit cell the displacements can be written in terms of top, bottom and interior displacements as shown in Fig. 8. Thus, the matrix problem can be reformulated in terms of top, bottom and interior displacements as

$$\begin{bmatrix} \boldsymbol{K}_{bb} & \boldsymbol{K}_{bI} & \boldsymbol{K}_{bt} \\ \boldsymbol{K}_{Ib} & \boldsymbol{K}_{II} & \boldsymbol{K}_{It} \\ \boldsymbol{K}_{tb} & \boldsymbol{K}_{tI} & \boldsymbol{K}_{tt} \end{bmatrix} \begin{Bmatrix} \boldsymbol{u}_b \\ \boldsymbol{u}_I \\ \boldsymbol{u}_t \end{Bmatrix} = \begin{Bmatrix} \boldsymbol{F}_b \\ \boldsymbol{F}_I \\ \boldsymbol{F}_t \end{Bmatrix} \tag{46}$$

In the above equation, the suffix b, I and t represent the top face, interior and bottom face of the unit cell, respectively. From Eq. (46) we can write,

$$\boldsymbol{K}_{II}\boldsymbol{u}_I + \boldsymbol{K}_{It}\boldsymbol{u}_t = \boldsymbol{F}_I - \boldsymbol{K}_{Ib}\boldsymbol{u}_b = \boldsymbol{F}_1 \tag{47}$$

and

$$\boldsymbol{K}_{tI}\boldsymbol{u}_I + \boldsymbol{K}_{tt}\boldsymbol{u}_t = \boldsymbol{F}_t - \boldsymbol{K}_{tb}\boldsymbol{u}_b = \boldsymbol{F}_2 \tag{48}$$

From Eq. (47), we can write $\boldsymbol{u}_I$ as

$$\boldsymbol{u}_I = \boldsymbol{K}_{II}^{-1}\boldsymbol{F}_1 - \boldsymbol{K}_{II}^{-1}\boldsymbol{K}_{It}\boldsymbol{u}_t \tag{49}$$

Substituting this in Eq. (48), we get

$$\boldsymbol{K}_{tI}\left(\boldsymbol{K}_{II}^{-1}\boldsymbol{F}_1 - \boldsymbol{K}_{II}^{-1}\boldsymbol{K}_{It}\boldsymbol{u}_t\right) + \boldsymbol{K}_{tt}\boldsymbol{u}_t = \boldsymbol{F}_2 \tag{50}$$

Rearranging the terms and representing

$$\boldsymbol{K}_{tt} - \boldsymbol{K}_{tI}\boldsymbol{K}_{II}^{-1}\boldsymbol{K}_{It} = \overline{\boldsymbol{K}}_{tt} \qquad \text{and} \qquad \boldsymbol{F}_2 - \boldsymbol{K}_{tI}\boldsymbol{K}_{II}^{-1}\boldsymbol{F}_1 = \overline{\boldsymbol{F}}_t \tag{51}$$

Eq. (50) can be rewritten as

$$\overline{\boldsymbol{K}}_{tt}\boldsymbol{u}_t = \overline{\boldsymbol{F}}_t \tag{52}$$

Solving Eq. (52) we get

$$\boldsymbol{u}_t = \overline{\boldsymbol{K}}_{tt}^{-1}\left(\boldsymbol{F}_2 - \boldsymbol{K}_{tI}\boldsymbol{K}_{II}^{-1}\boldsymbol{F}_1\right) \tag{53}$$

Substituting the values of $\boldsymbol{F}_1$ and $\boldsymbol{F}_2$ from Eq. (47), we get

$$\boldsymbol{u}_t = \overline{\boldsymbol{K}}_{tt}^{-1}\left[\boldsymbol{F}_t - \boldsymbol{K}_{tb}\boldsymbol{u}_b - \boldsymbol{K}_{tI}\boldsymbol{K}_{II}^{-1}(\boldsymbol{F}_I - \boldsymbol{K}_{Ib}\boldsymbol{u}_b)\right] \tag{54}$$

Substituting, $\overline{\overline{\boldsymbol{F}}} = \overline{\boldsymbol{K}}_{tt}^{-1}(\boldsymbol{F}_t - \boldsymbol{K}_{tI}\boldsymbol{K}_{II}^{-1}\boldsymbol{F}_I)$ and $\overline{\overline{\boldsymbol{K}}} = \overline{\boldsymbol{K}}_{tt}^{-1}(\boldsymbol{K}_{tI}\boldsymbol{K}_{II}^{-1}\boldsymbol{K}_{Ib} - \boldsymbol{K}_{tb})$, the final equation can be written as,

$$\boldsymbol{u}_t = \overline{\overline{\boldsymbol{F}}} + \overline{\overline{\boldsymbol{K}}}\boldsymbol{u}_b \tag{55}$$

From Eq. (55), we can extract the displacements in the vicinity of the boundary, as one moves from the boundary to the interior of the domain. Note that since $\boldsymbol{F}_t, \boldsymbol{F}_I = 0$, Eq. (55) leads to the recursive relation $\boldsymbol{u}_t = \overline{\overline{\boldsymbol{K}}}\boldsymbol{u}_b$. This gives us

$$\boldsymbol{u}_t^{(i)} = \overline{\overline{\boldsymbol{K}}}^{(i)}\boldsymbol{u}_t^{(0)} \tag{56}$$

As $\overline{\overline{\boldsymbol{K}}}$ is invertible, from diagonalization we can write,

$$\overline{\overline{\boldsymbol{K}}} = [P][\Lambda][P]^{-1} \tag{57}$$

For the ith term we get,

$$\overline{\overline{\boldsymbol{K}}}^{(i)} = [P][\Lambda]^{(i)}[P]^{-1} \tag{58}$$

Thus, Eq. (56) can be rewritten as,

$$\boldsymbol{u}_t^{(i)} = [P][\Lambda]^{(i)}[P]^{-1}\boldsymbol{u}_t^{(0)} \tag{59}$$

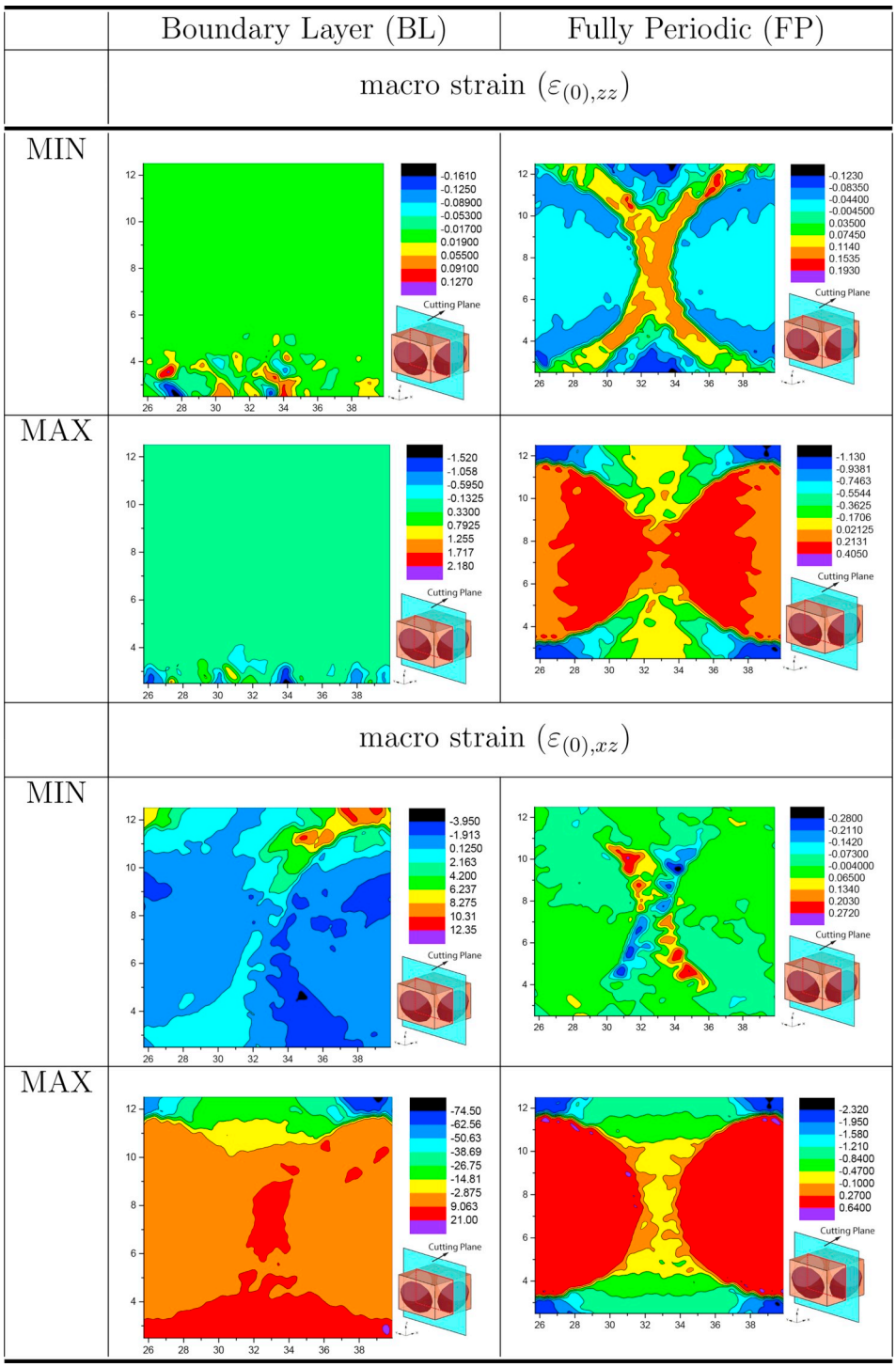

Fig. 18. Comparison of micro strain for BL and FP problem - normal and shear load cases for 45° RVE.

Table 9
Extreme values of micro strains for applied shear macro strain for both boundary layer (BL) and fully periodic (FP) problems for RVE with 45° fibre orientation.

Macro Strain		$\varepsilon_{(0),yz}$		$\varepsilon_{(0),xz}$		$\varepsilon_{(0),xy}$	
		BL	FP	BL	FP	BL	FP
|Strain Value|	MIN	0.44	0.278	3.95	0.272	0.08	0.104
	MAX	18	2.300	74.50	2.320	2.06	0.624
Strain Type	MIN	$\varepsilon_{zz}^{(bl)}$	$\varepsilon_{(1),zz}$	$\varepsilon_{zz}^{(bl)}$	$\varepsilon_{(1),zz}$	$\varepsilon_{xx}^{(bl)}$	$\varepsilon_{(1),zz}$
	MAX	$\varepsilon_{xz}^{(bl)}$	$\varepsilon_{(1),yz}$	$\varepsilon_{xz}^{(bl)}$	$\varepsilon_{(1),xz}$	$\varepsilon_{zz}^{(bl)}$	$\varepsilon_{(1),xy}$

which upon pre-multiplying by $[P]^{-1}$ gives

$$[P]^{-1}\boldsymbol{u}_t^{(i)} = [\Lambda]^{(i)}[P]^{-1}\boldsymbol{u}_t^{(0)} \tag{60}$$

or,

$$\boldsymbol{y}_t^{(i)} = [\Lambda]^{(i)}\boldsymbol{y}_t^{(0)} \quad \text{where,} \quad \boldsymbol{y}_t^{(i)} = [P]^{-1}\boldsymbol{u}_t^{(i)} \quad \text{and} \quad \boldsymbol{y}_t^{(0)} = [P]^{-1}\boldsymbol{u}_t^{(0)} \tag{61}$$

Letting each term be given as, $\boldsymbol{y}_{t_k}^{(i)} = \boldsymbol{y}_{t_k}^{(0)} e^{-i/t_k}$ we get,

Table 10
Extreme values of micro stresses for applied normal macro strain for both boundary layer (BL) and fully periodic (FP) problems for RVE with 0° fibre orientation.

Macro Strain		$\varepsilon_{(0),xx}$		$\varepsilon_{(0),yy}$		$\varepsilon_{(0),zz}$	
		BL	FP	BL	FP	BL	FP
|Stress Value|	MIN	7.05	6.50	244	465	560	405
	MAX	76.50	108	1910	7900	4800	7900
Stress Type	MIN	$\sigma_{xz}^{(bl)}$	$\sigma_{(1),xz}$	$\sigma_{xz}^{(bl)}$	$\sigma_{(1),xz}$	$\sigma_{xz}^{(bl)}$	$\sigma_{(1),xz}$
	MAX	$\sigma_{yy}^{(bl)}$	$\sigma_{(1),xx}$	$\sigma_{yy}^{(bl)}$	$\sigma_{(1),yy}$	$\sigma_{yy}^{(bl)}$	$\sigma_{(1),zz}$

$$\boldsymbol{y}_{t_k}^{(i)} = \boldsymbol{y}_{t_k}^{(0)} \left(e^{-1/t_k}\right)^i = \boldsymbol{y}_{t_k}^{(0)} \lambda_k^i \tag{62}$$

where, $\lambda_k = e^{-1/t_k}$. Considering the norm of the nodal displacements, we can write

$$\left\|\boldsymbol{y}_t^{(i)}\right\| \approx \left\|\boldsymbol{y}_t^{(0)}\right\| e^{-i/t_k} \approx \left\|\boldsymbol{y}_t^{(i)}\right\| (\lambda)^i \tag{63}$$

It is noticed that the exponential decay perfectly matches with the displacement norms, as shown in the numerical results later. We will also show that the decay of boundary-layer depends on the strain and material. The method of this section can thus be used to study boundary-layers for any boundary condition and (periodic) material.

6. Numerical results

To illustrate the method given in the previous section, some numerical results are presented. To study these effects, three different cell geometries are considered for unidirectional fibre reinforced composites with fibres orientated at 0^0, 45^0 and 90^0 as shown in Fig. 9.

By using the required information three dimensional representative volume element (RVE) models are generated in ABAQUS/Standard, which are then imported in HYPERMESH software for meshing. Initially, solid RVE is meshed on one side of the surface of cube using two dimensional (2D) triangular elements and then same elements get duplicated and translated to the opposite face to maintain periodicity. Three dimensional (3D) linear tetrahedron matrix and fibre elements are created, which now represent an RVE with finite elements. All the three finite element (FE) models are generated with approximately 2609 nodes and 11121 elements, as shown in Fig. 9. Once the meshing is over, the mesh data like, the total number of elements, total number of nodes, their coordinates and node connectivity, is extracted. These are given as input to the mathematical homogenization code, which is written in FORTRAN 77. In this study, unidirectional composite laminate composed of epoxy matrix and carbon fibre is considered. The constituent material for matrix and fibre are assumed as isotropic and transversely isotropic, respectively. Tables 1 and 2 give the material properties used in this study.

The focus of these analyses is to study the longitudinal, transverse and shear behaviour of the material and also to determine how the boundary layer decays from the fixed edge to the interior of the domain in the y_3 direction. Note that on the $y_1 - y_3$ and $y_2 - y_3$ planes the periodicity of $\boldsymbol{u}^{(bl)}$ is enforced. In this boundary layer analysis, the above mentioned FE models are considered with non - periodicity boundary condition in the depth direction.

6.1. Decay of displacement for RVEs with fibre orientations 0°, 45° and 90°

For the above analyses, the norms are calculated for different fibre orientation, i.e. 0°, 45° and 90° RVE. L_2 - norm of nodal displacements for each of the displacement component is used as a measure. Here, L_2 - norm is defined as

$$\|\boldsymbol{x}\|_{L_2} = \sqrt{\sum_i x_i^2} \tag{64}$$

The problem is solved by applying unit macro strain on these finite element models. It is observed that the displacement norms are settling within five to six layers along the thickness direction. However, for each fibre orientation the magnitude of the displacement norm varies significantly for normal and shear load cases. Fig. 10 and Fig. 11 show the plots of the decay of the displacement norms for different fibre orientation from Face/layer 2 to 7. The figures clearly demonstrate that the displacement norm settles quickly, for different loading conditions.

From Table 3, it can also be seen that for 0° fibre orientation the minimum and the maximum norm occur for v displacement and for 90° fibre orientation both of these norms occur for u displacement. However, minimum and maximum displacement norm for 45° RVE are for w and v displacements, respectively. For the shear load case, the maximum value is $7.54E-01$ for macro strain of $\varepsilon_{(0),yz}$ for 0° RVE. Even the maximum values for the other shear load cases are $5.42E-01$ for $\varepsilon_{(0),yz}$ for 45° RVE and $2.85E-02$ for $\varepsilon_{(0),xy}$ for 0° RVE.

Interestingly, note that the minimum norm values for all the three orientations occur for the macro normal load conditions but the maximum norm values occur for the macro shear load case, mainly for $\varepsilon_{(0),yz}$ loading condition. This means that the boundary layer tail has a significant effect for $\varepsilon_{(0),yz}$ macro strain. From Table 3, it can be seen that the maximum norms are decaying in 5–6 layers for 45° and 90° RVEs. For 0° RVE the maximum norm is settling down in 6–7 layers. Note that for all the three different fibre orientations, boundary layer due to shear load is significant.

To show the theoretically desired (refer to Saint-Venant's principle based on Hill-Yosida theorem) exponential decay by means of curve fitting, we get the equation which is of the form

$$y \approx Ae^{-z/t} \tag{65}$$

where, z is the distance along the strip and t is the decay factor or characteristic length. For studying the exponential decay of the displacement fields, we considered the plots from Face 2 to Face 7 for the above mentioned maximum displacement norms. Fig. 12 shows the exponential decay of the displacement norms for macro strain $\varepsilon_{(0),yz}$ for RVE with 0° fibre orientation.

In Fig. 12, the table shows the values of the constants of Eq. (65) for different displacement norms for $\varepsilon_{(0),yz}$ macro strains. Fig. 13 shows the exponential decay of the maximum displacement norms for macro strain $\varepsilon_{(0),yz}$ for RVE with 45° fibre orientation. In Fig. 13, table shows the constant values of the exponential decay for the RVE with 45° fibre

Table 11
Extreme values of micro stresses for applied shear macro strain for both boundary layer (BL) and fully periodic (FP) problems for RVE with 0° fibre orientation.

Macro Strain		$\varepsilon_{(0),yz}$		$\varepsilon_{(0),xz}$		$\varepsilon_{(0),xy}$	
		BL	FP	BL	FP	BL	FP
|Stress Value|	MIN	3720	410	1660	182	1760	155
	MAX	3.04E04	4320	9750	1.07E04	1.70E04	1.07E04
Stress Type	MIN	$\sigma_{yz}^{(bl)}$	$\sigma_{(1),xz}$	$\sigma_{xy}^{(bl)}$	$\sigma_{(1),yz}$	$\sigma_{yz}^{(bl)}$	$\sigma_{(1),yz}$
	MAX	$\sigma_{xx}^{(bl)}$	$\sigma_{(1),yz}$	$\sigma_{xx}^{(bl)}$	$\sigma_{(1),xz}$	$\sigma_{xx}^{(bl)}$	$\sigma_{(1),xy}$

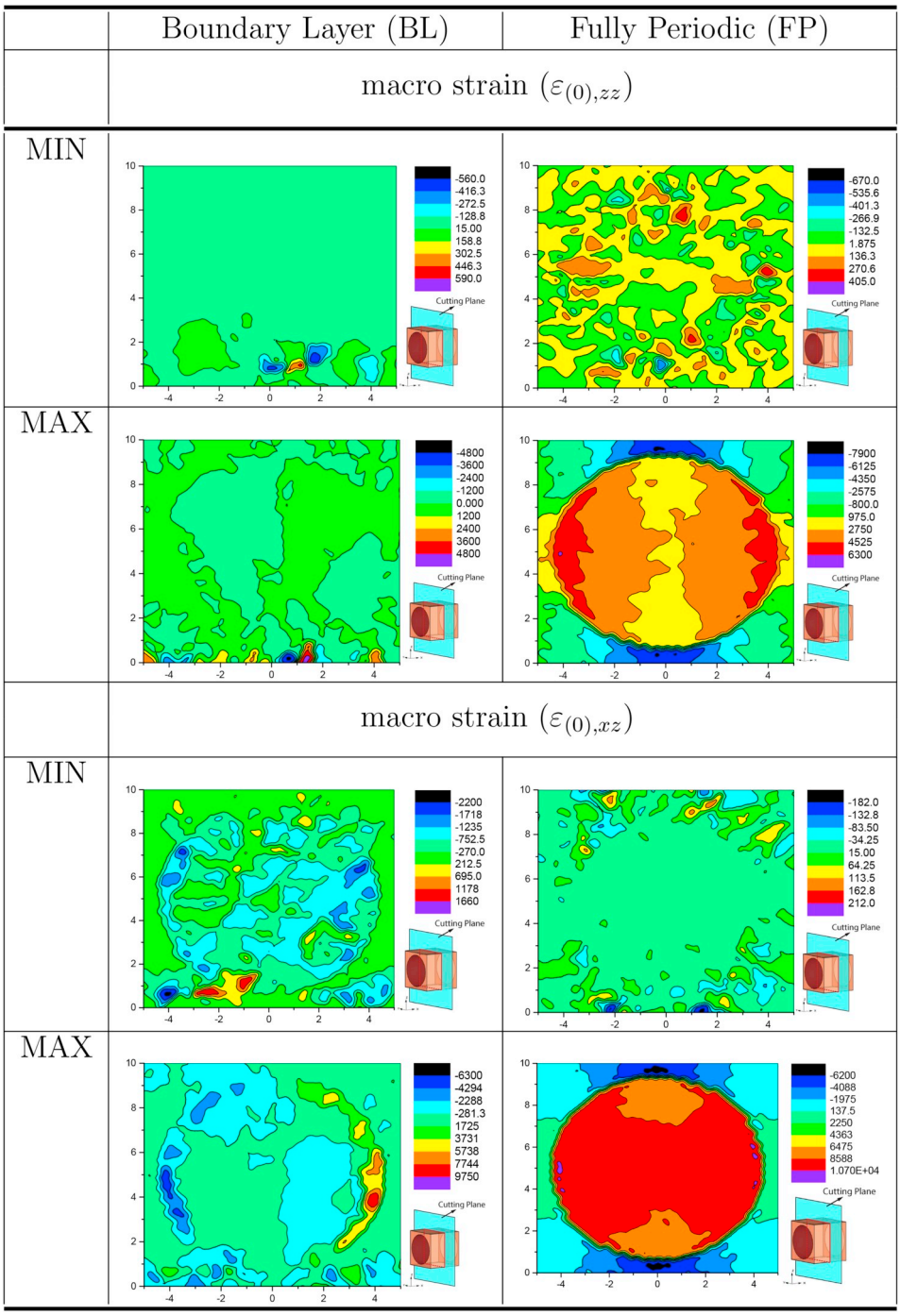

Fig. 19. Comparison of micro stress for BL and FP problem - normal and shear load cases for 0° RVE.

Table 12
Extreme values of micro stresses for applied normal macro strain for both boundary layer (BL) and fully periodic (FP) problems for RVE with 90° fibre orientation.

Macro Strain		$\varepsilon_{(0),xx}$		$\varepsilon_{(0),yy}$		$\varepsilon_{(0),zz}$	
		BL	FP	BL	FP	BL	FP
|Stress Value|	MIN	10.3	120	425	5900	292	9000
	MAX	98	6400	2370	7.35*E*05	6050	2.50*E*05
Stress Type	MIN	$\sigma_{xz}^{(bl)}$	$\sigma_{(1),xx}$	$\sigma_{yz}^{(bl)}$	$\sigma_{(1),xz}$	$\sigma_{xz}^{(bl)}$	$\sigma_{(1),xx}$
	MAX	$\sigma_{xx}^{(bl)}$	$\sigma_{(1),yy}$	$\sigma_{zz}^{(bl)}$	$\sigma_{(1),yy}$	$\sigma_{yy}^{(bl)}$	$\sigma_{(1),yy}$

Table 13
Extreme values of micro stresses for applied shear macro strain for both boundary layer (BL) and fully periodic (FP) problems for RVE with 90° fibre orientation.

Macro Strain		$\varepsilon_{(0),yz}$		$\varepsilon_{(0),xz}$		$\varepsilon_{(0),xy}$	
		BL	FP	BL	FP	BL	FP
|Stress Value|	MIN	1180	1.68*E*04	3080	430	1060	590
	MAX	7.60*E*04	9.20*E*05	4.60*E*04	1.36*E*05	2.44*E*04	1.28*E*05
Stress Type	MIN	$\sigma_{xy}^{(bl)}$	$\sigma_{(1),xx}$	$\sigma_{xz}^{(bl)}$	$\sigma_{(1),yz}$	$\sigma_{yz}^{(bl)}$	$\sigma_{(1),yz}$
	MAX	$\sigma_{xx}^{(bl)}$	$\sigma_{(1),yy}$	$\sigma_{yz}^{(bl)}$	$\sigma_{(1),xy}$	$\sigma_{xx}^{(bl)}$	$\sigma_{(1),xy}$

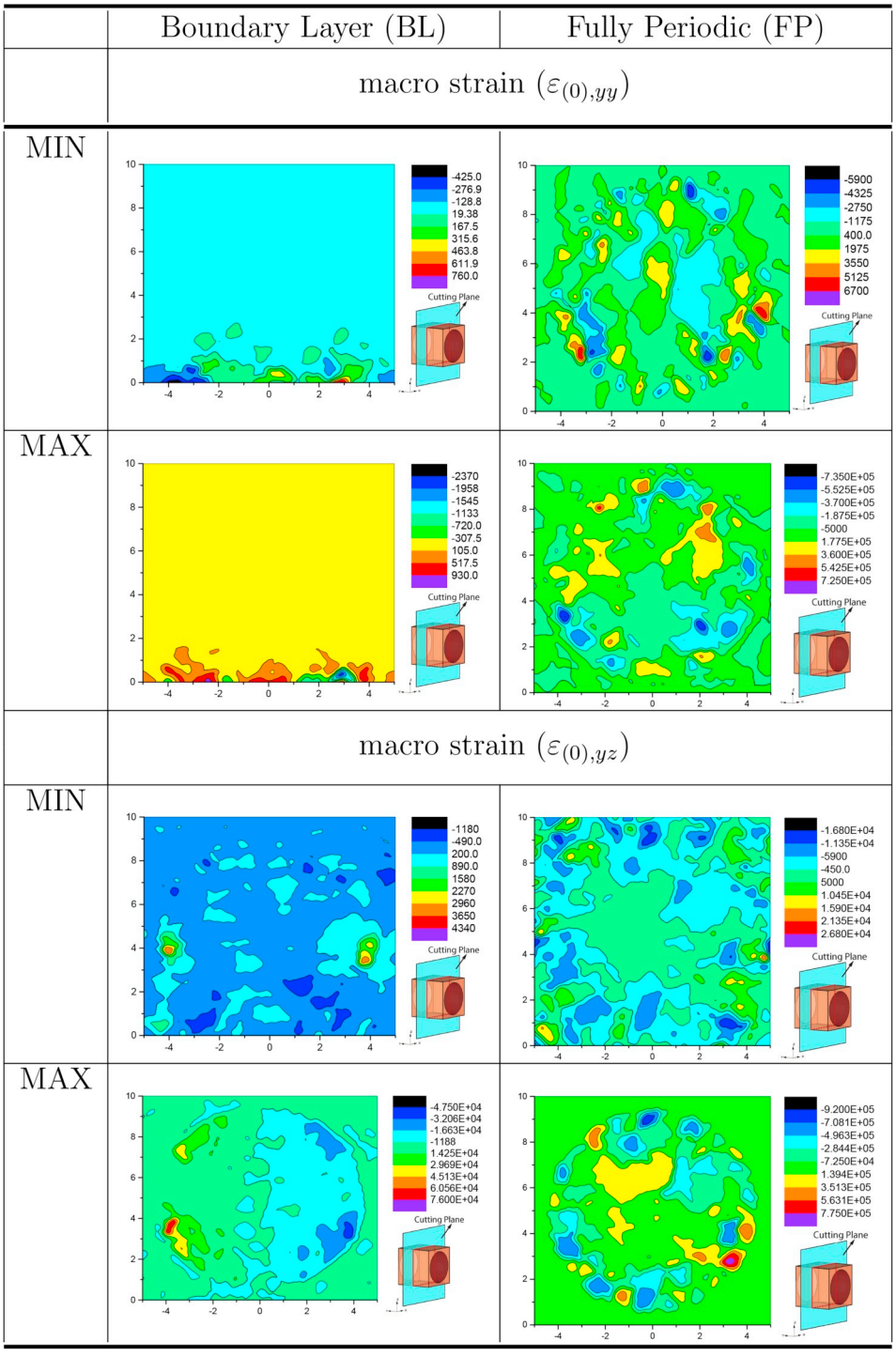

Fig. 20. Comparison of micro stress for BL and FP problem - normal and shear load cases for 90° RVE.

Table 14
Extreme values of micro stresses for applied normal macro strain for both boundary layer (BL) and fully periodic (FP) problems for RVE with 45° fibre orientation.

Macro Strain		$\varepsilon_{(0),xx}$		$\varepsilon_{(0),yy}$		$\varepsilon_{(0),zz}$	
		BL	FP	BL	FP	BL	FP
|Stress Value|	MIN	1960	1480	1620	1160	1100	550
	MAX	1.40*E*04	1.50*E*04	1.52*E*04	1.76*E*04	1.08*E*04	9550
Stress Type	MIN	$\sigma_{yz}^{(bl)}$	$\sigma_{(1),yz}$	$\sigma_{yz}^{(bl)}$	$\sigma_{(1),xz}$	$\sigma_{xz}^{(bl)}$	$\sigma_{(1),xy}$
	MAX	$\sigma_{xx}^{(bl)}$	$\sigma_{(1),xx}$	$\sigma_{xx}^{(bl)}$	$\sigma_{(1),yy}$	$\sigma_{xx}^{(bl)}$	$\sigma_{(1),xy}$

Table 15
Extreme values of micro stresses for applied shear macro strain for both boundary layer (BL) and fully periodic (FP) problems for RVE with 45° fibre orientation.

Macro Strain		$\varepsilon_{(0),yz}$		$\varepsilon_{(0),xz}$		$\varepsilon_{(0),xy}$	
		BL	FP	BL	FP	BL	FP
|Stress Value|	MIN	1.34*E*04	2020	4.20*E*04	2000	2680	505
	MAX	6.10*E*04	7450	1.12*E*06	7500	1.33*E*04	1.38*E*04
Stress Type	MIN	$\sigma_{zz}^{(bl)}$	$\sigma_{(1),xz}$	$\sigma_{yz}^{(bl)}$	$\sigma_{(1),yz}$	$\sigma_{xy}^{(bl)}$	$\sigma_{(1),yz}$
	MAX	$\sigma_{yy}^{(bl)}$	$\sigma_{(1),yz}$	$\sigma_{xx}^{(bl)}$	$\sigma_{(1),xz}$	$\sigma_{zz}^{(bl)}$	$\sigma_{(1),xy}$

Further, it is to be noted that stress values are much higher for the shear condition compared to the normal cases.

orientation.

Similarly, Fig. 14 shows the exponential decay of the maximum displacement norms for macro strain $\varepsilon_{(0),yz}$ for RVE with 90° fibre orientation. In Fig. 14, table shows the constant values of the exponential decay for the RVE with 90° fibre orientation.

It is observed that after doing the curve fitting, the exponential decay plot converges with the norm plot (with the value of R^2 above 0.99) for all the load cases. Importantly, it should be noted that the coefficients (for the exponential decay) depend strongly on the load type and fibre orientation.

6.2. Variation of micro strains along the depth of the RVE

In this section, we will study the variation of micro strains along the depth of an RVE for both boundary layer (BL) and fully periodic (FP) problems. Here, RVEs with 0°, 45° and 90° fibre orientations are studied. The planes on which the micro strains distribution is obtained are shown in Fig. 15 for these RVEs. For 0° and 45° RVEs the planes are midway along x - axis and for 90° RVE it is midway along y - axis.

The variation of micro strains and micro stresses are estimated for all the three macro normal strains $\varepsilon_{(0),jj}$ and macro shear strains $\varepsilon_{(0),ij}$. Note that the bar on the symbol for macro strain, asterisk for both boundary layer microstrain and fully periodic microstrain (as in Eq. (34)) are omitted for brevity in the following. Illustrative contour plots are presented, for both minimum and maximum micro strain and stress, only for one normal macro strain and one shear macro strain cases.

6.2.1. Variation of micro strains along the depth of the RVE for 0° fibre orientation

For macro normal strain load cases, the minimum and maximum values of micro strains and their types, for boundary layer and fully periodic problems are reported in Table 4. Further, the corresponding micro strain distributions on a plane perpendicular to x - axis at mid length of x - axis through contour plots are shown in Fig. 16. The plane on which the contours are plotted is also depicted in these figures. From the results, it can be seen that in comparison to the boundary layer problem, the micro strain values for all the macro strains are higher for fully periodic problem except for $\varepsilon_{(0),xx}$. Furthermore, it can be observed that for macro normal cases, the maximum micro strains for fully periodic problem occur in normal micro strain components whereas for boundary layer problem the maximums occur for shear micro strains.

From Table 5, we see that for macro shear strains the maximum of maximum and minimum values in micro strains are obtained for the boundary layer problem. However, the nature of the micro strains for which these values are obtained differ for boundary layer as compared to the fully periodic problem. The minimum values are obtained only for normal micro strains. In contrast, maximum value is obtained for shear micro strains.

Thus, for this particular fibre orientation, shear load cases have significant effect due to boundary layer. Furthermore, it can be observed that for fully periodic cases with macro shear strains the maximum values are also reported for the same nature of micro strains, that is for $\varepsilon_{(0),yz}$ the maximum value is seen for $\varepsilon_{(1),yz}$ and likewise. However, for boundary layer problem these micro strain components are different than macro strain cases.

6.2.2. Variation of micro strains along the depth of the RVE for 90° fibre orientation

The minimum and maximum values of micro strains and their types in this RVE, for boundary layer and fully periodic problems are reported in Table 6 for normal macro strain. Further, the corresponding micro strain distributions on a plane perpendicular to y - axis at mid length of y - axis (as shown in Fig. 15) through contour plots are shown in Fig. 17. For the 90° RVE, it has been observed that $\varepsilon_{xx}^{(bl)}$ has the lowest value for the boundary layer problem among all the normal load cases. From Table 6, it can be observed that for $\varepsilon_{(0),yy}$ and $\varepsilon_{(0),zz}$ the maximum strain values are respectively 10 and 4 times higher for fully periodic problem compared to boundary layer. Also, in all macro strain cases it occurs for the micro strain $\varepsilon_{(1),yz}$. Thus, it is an important result that for the macro normal load cases micro strain $\varepsilon_{(1),yz}$ is significantly effected by the boundary layer correction, with a lowering of the actual strain. Further, it is important to see that except $\varepsilon_{(0),xx}$ for boundary layer problem, the macro normal strains affect the micro shear strains.

The results due to macro shear load cases are reported in Table 7. It is noticed from Tables 6 and 7 that the minimum strain value of both the normal and shear load cases for boundary layer and fully periodic problem occurs in micro normal strains only. For all shear load cases, the maximum strain value for boundary layer and fully periodic problem occurs for micro shear strains. It can also be noticed that the maximum value is 29.2 for $\varepsilon_{yz}^{(bl)}$ for $\varepsilon_{(0),xz}$ which is significantly higher compared to other strain values. Further, for $\varepsilon_{(0),yz}$ and $\varepsilon_{(0),xy}$ the maximum values of micro strains have significant differences.

Thus, from the above discussion it can be noted that the normal and

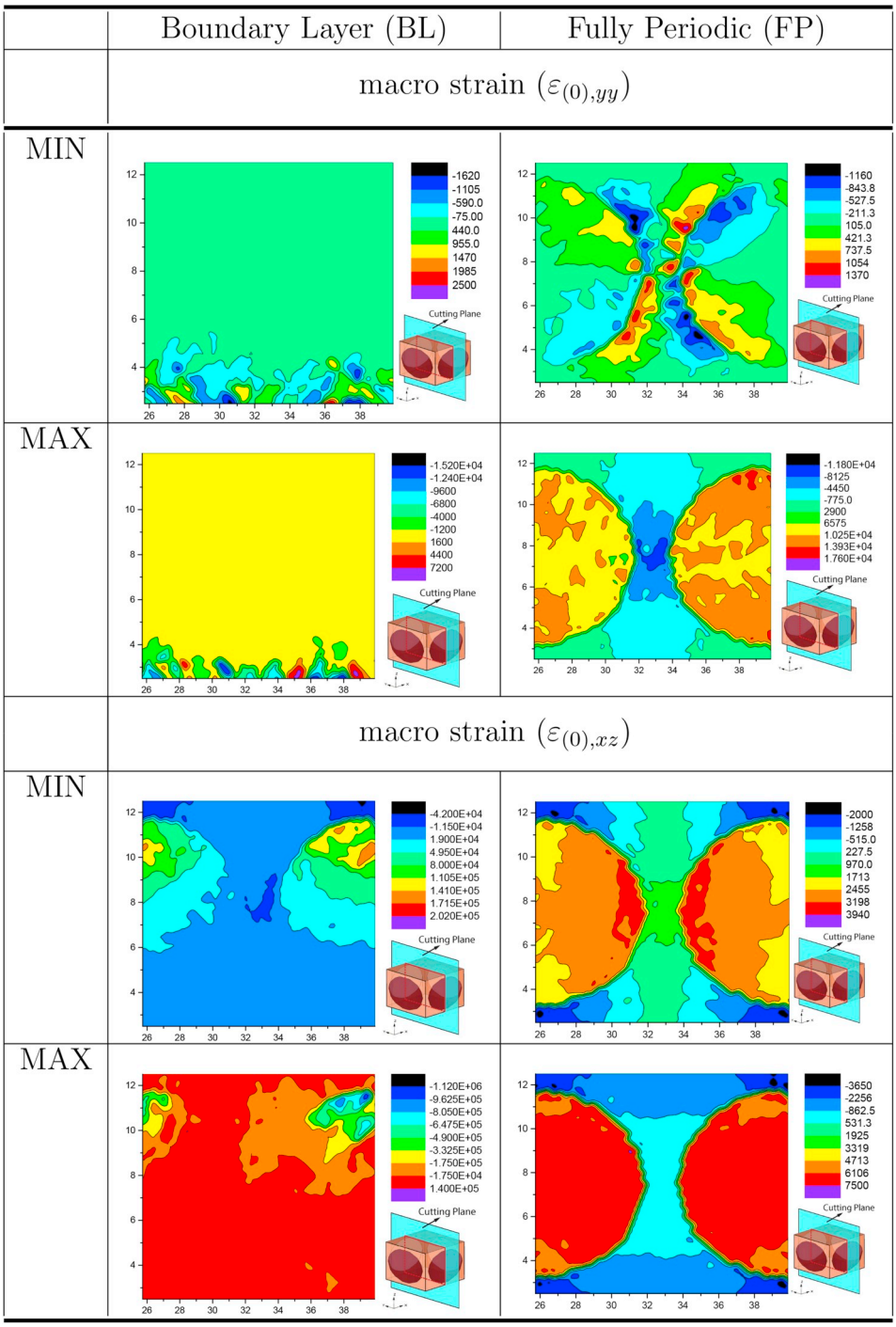

Fig. 21. Comparison of micro stress for BL and FP problem - normal and shear load cases for 45° RVE.

Table 16
Variation of σ_{RMS} along the depth of the RVEs for both boundary layer (BL) and fully periodic (FP) problems considering normal macro strain.

Macro Strain	$\varepsilon_{(0),xx}$		$\varepsilon_{(0),yy}$		$\varepsilon_{(0),zz}$	
	BL	FP	BL	FP	BL	FP
0° RVE	8.917*E*02	2.084*E*03	1.139*E*04	7.092*E*03	2.101*E*04	5.399*E*03
90° RVE	2.966*E*03	5.483*E*03	9.102*E*04	1.850*E*03	1.583*E*05	4.664*E*03
45° RVE	6.101*E*05	3.390*E*04	7.229*E*05	3.385*E*04	4.383*E*05	1.928*E*04

Table 17
Variation of σ_{RMS} along the depth of the RVEs for both boundary layer (BL) and fully periodic (FP) problems considering shear macro strain.

Macro Strain	$\varepsilon_{(0),yz}$		$\varepsilon_{(0),xz}$		$\varepsilon_{(0),xy}$	
	BL	FP	BL	FP	BL	FP
0° RVE	7.872*E*06	7.479*E*03	3.440*E*05	1.878*E*04	4.632*E*05	1.885*E*04
90° RVE	3.001*E*05	2.006*E*04	2.514*E*07	7.513*E*03	1.107*E*05	1.895*E*04
45° RVE	1.208*E*07	1.562*E*04	3.087*E*07	1.535*E*04	1.423*E*05	2.594*E*04

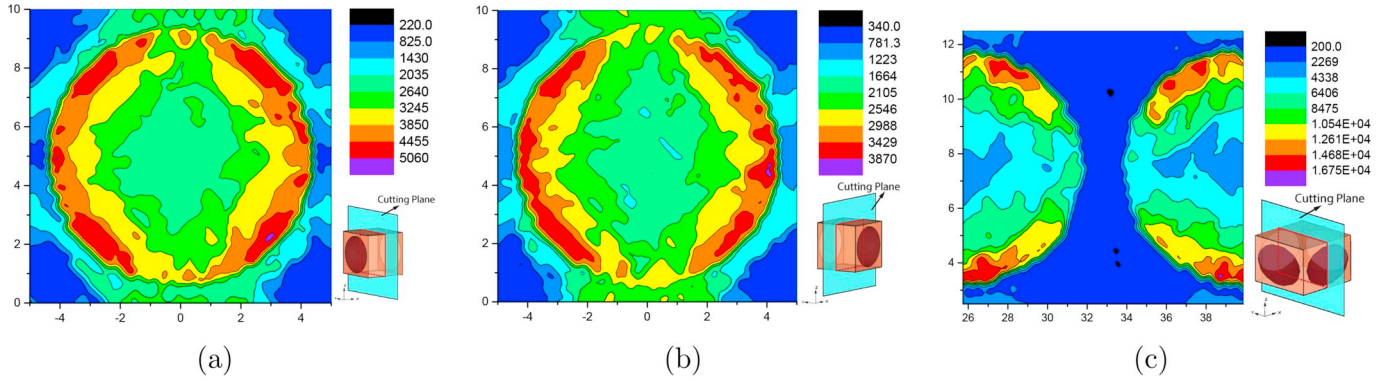

Fig. 22. Distribution of σ_{RMS} for macro strain ($\varepsilon_{(0),zz}$) for fully periodic problem (FP). (a) RVE with 0° fibre orientation, (b) RVE with 90° fibre orientation, (c) RVE with 45° fibre orientation.

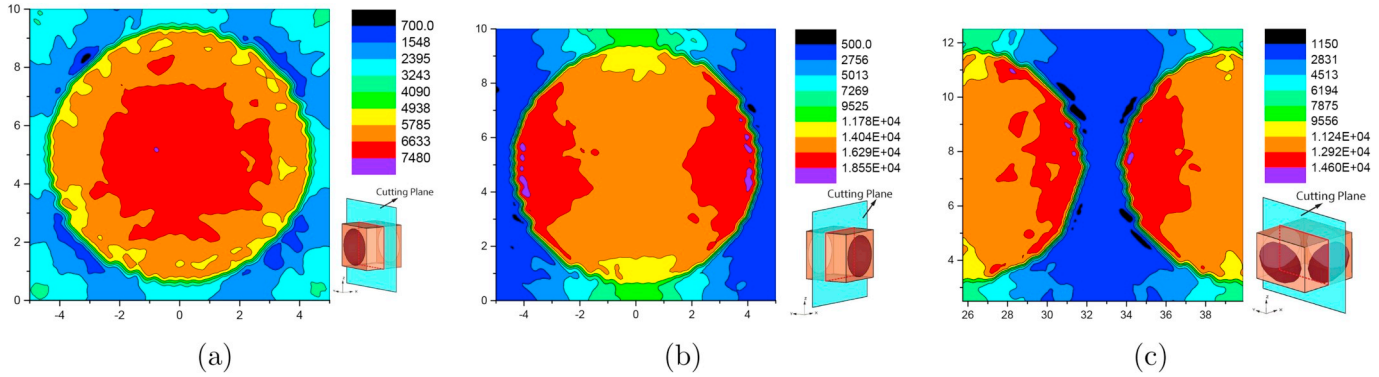

Fig. 23. Distribution of σ_{RMS} for macro strain ($\varepsilon_{(0),yz}$) for fully periodic problem (FP). (a) RVE with 0° fibre orientation, (b) RVE with 90° fibre orientation, (c) RVE with 45° fibre orientation.

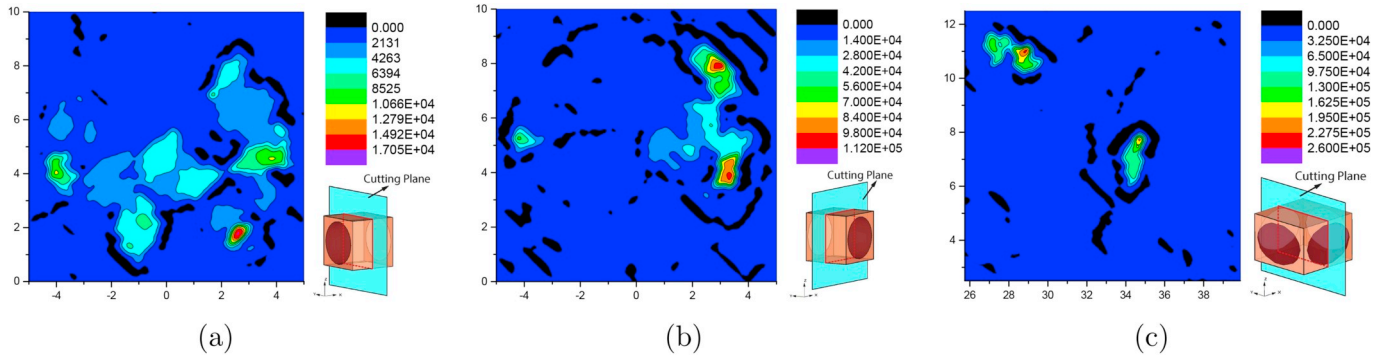

Fig. 24. Distribution of σ_{RMS} for macro strain ($\varepsilon_{(0),zz}$) for boundary layer problem (BL). (a) RVE with 0° fibre orientation, (b) RVE with 90° fibre orientation, (c) RVE with 45° fibre orientation.

shear load cases have significantly different effects for fully periodic and boundary layer problems. It is also observed that micro strain $\varepsilon_{yz}^{(bl)}$ has significant effect due to boundary layer.

6.2.3. Variation of micro strains along the depth of the RVE for 45° fibre orientation

For this particular fibre orientation, the minimum and maximum

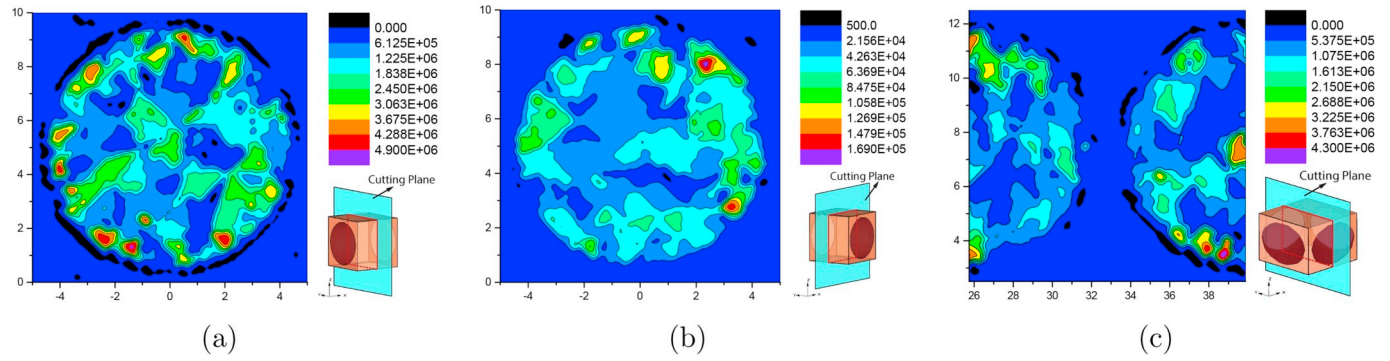

Fig. 25. Distribution of σ_{RMS} for macro strain ($\varepsilon_{(0),yz}$) for boundary layer problem (BL). (a) RVE with 0 fibre orientation, (b) RVE with 90° fibre orientation, (c) RVE with 45° fibre orientation.

Table 18
Variation of maximum σ_{RMS} along the fibre-matrix interface for both boundary layer (BL), fully periodic (FP) problems for RVE with 0° fibre orientation.

Macro Strain	$\varepsilon_{(0),xx}$	$\varepsilon_{(0),yy}$	$\varepsilon_{(0),zz}$	$\varepsilon_{(0),yz}$	$\varepsilon_{(0),xz}$	$\varepsilon_{(0),xy}$
Boundary layer (BL) problem	40.726	2015.783	2351.362	125126.904	29932.831	11093.059
Fully periodic (FP) problem	47.261	4509.979	2904.696	3183.566	10605.603	10512.138
Ratio (BL/FP)	0.862	0.447	0.810	39.304	2.822	1.055

Table 19
Variation of maximum σ_{RMS} along the fibre-matrix interface for both boundary layer (BL), fully periodic (FP) problems for RVE with 90° fibre orientation.

Macro Strain	$\varepsilon_{(0),xx}$	$\varepsilon_{(0),yy}$	$\varepsilon_{(0),zz}$	$\varepsilon_{(0),yz}$	$\varepsilon_{(0),xz}$	$\varepsilon_{(0),xy}$
Boundary layer (BL) problem	22.333	1148.409	1428.395	21506.160	204189.102	8215.585
Fully periodic (FP) problem	3609.071	41.138	2641.533	10683.544	3220.292	10545.845
Ratio (BL/FP)	0.006	27.916	0.541	2.013	63.407	0.779

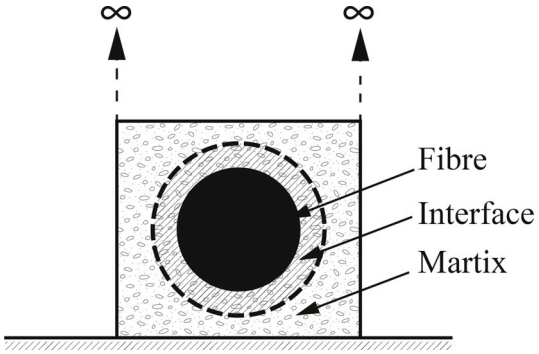

Fig. 26. Unit cell representing the fibre-matrix interface where the maximum σ_{RMS} value is extracted.

values of micro strains and their types, for boundary layer and fully periodic problems are reported in Table 8 for normal macro strain. Further, the variation of micro strains are observed through contour plots which are shown in Fig. 18. Both normal and shear macro strains are applied on the RVE for both boundary layer and fully periodic problems. Here, for all the cases the maximum value occurs for boundary layer problem. Further, for all macro normal load cases, it can be observed that the maximum value among all the micro strain is for $\varepsilon_{xy}^{(bl)}$ but for the fully periodic problem the maximum strain value occurs for the micro normal strain corresponding to a macro strain applied (see Table 8).

The minimum and maximum values of micro strains and their types, for boundary layer and fully periodic problems are reported in Table 9 for macro shear strains. For $\varepsilon_{(0),yz}$ and $\varepsilon_{(0),xz}$ the maximum strain value occurs for $\varepsilon_{xz}^{(bl)}$ with values 18 and 74.5, respectively which is much higher compared to the micro strain for fully periodic problem. However, for $\varepsilon_{(0),xy}$ maximum strain value occurs for $\varepsilon_{zz}^{(bl)}$. For the fully periodic problem, the maximum value occurs for micro strain types corresponding to macro strain. For example, for $\varepsilon_{(0),yz}$ it occurs for $\varepsilon_{(1),yz}$.

Thus, for this particular fibre orientation it can be noticed that both for normal and shear macro strain the maximum strain value occurs only for the micro shear strains mainly in the boundary layer problem. So, it can be concluded that boundary layer significantly affects the shear micro strains, mainly $\varepsilon_{(1),xz}$.

6.3. Variation of micro stresses along the depth of the RVE

In this section, we will study the variation of micro stresses along the depth of an RVE for both boundary layer (BL) and fully periodic (FP) problems. Here, RVEs with 0°, 45° and 90° fibre orientations are studied.

6.3.1. Variation of micro stresses along the depth of the RVE for 0° fibre orientation

The variation of micro stresses has been also observed due to applied macro strains on the RVE. The variation of micro stresses due to applied macro strains is reported in Table 10 and Table 11 for normal and shear macro strains, respectively. Further, the corresponding distribution of these micro stresses on planes as shown in Fig. 15 is shown in Fig. 19 for normal and shear macro strains, respectively. It can be noticed that for

the normal macro strains the maximum stress values are much higher for the fully periodic problem compared to boundary layer corrected case. These values are 2–4 times more than corresponding boundary layer problem values. From Table 10, it can be noticed that the maximum stress value for the boundary layer case occurs for $\sigma_{yy}^{(bl)}$ whereas for the fully periodic case the maximum stress value occurs corresponding to applied macro strain, i.e. for $\varepsilon_{(0),jj}$ it is $\sigma_{(1),jj}$. Further, it is interesting to note that the minimum value occurs for σ_{xz} component for all normal macro strain cases in both boundary layer and fully periodic problems.

For the macro shear load cases, it can be observed that the maximum stress value is for $\sigma_{xx}^{(bl)}$ for all the three applied macro shear strains. Further, from Table 11 it is observed that $\sigma_{xx}^{(bl)}$ has the maximum stress value for unit macro strain of $\varepsilon_{(0),yz}$. However, for the fully periodic case it can be noticed from Table 11 that maximum stress value occurs for the corresponding shear micro strains, i.e. for $\varepsilon_{(0),ij}$ the stresses are $\sigma_{(1),ij}$.

Thus, from these results it can be concluded that stress values are maximum for the boundary layer case as compared to fully periodic for the macro shear load case. However, for the macro normal load cases the maximum reduces when boundary layer correction is made.

6.3.2. *Variation of micro stresses along the depth of the RVE for 90° fibre orientation*

The minimum and maximum values of micro stresses and their types, for boundary layer and fully periodic problems are obtained for this RVE and reported in Table 12 and Table 13 for macro normal and shear strains, respectively. The variation of micro stresses is given as contour plots in Fig. 20. From Table 12, it can be noticed that the stress values are maximum for the fully periodic problem when macro normal loads are applied. Interestingly, from Table 12 it can be seen that the maximum stress occurs for $\sigma_{(1),yy}$ for all the three macro normal strains for the fully periodic case. However, for the boundary layer case, the maximum value depends on the applied macro strain. It is noteworthy that for $\varepsilon_{(0),yy}$ and $\varepsilon_{(0),zz}$ the maximum stress for the fully periodic case is much higher compared to the boundary layer solution.

From Table 13 it is seen that for the macro shear load condition, the maximum stress occurs for fully periodic case. The maximum value observed is $\sigma_{(1),yy}$ for fully periodic case when $\varepsilon_{(0),yz}$ is applied. Further, it is seen that the maximum stress value occurs for $\sigma_{xx}^{(bl)}$ for both the macro strain $\varepsilon_{(0),yz}$ and $\varepsilon_{(0),xy}$ for the boundary layer case but for the fully periodic problem it occurs for $\sigma_{(1),xy}$. Interestingly, the boundary layer correction reduces the micro-stress intensity for this case.

It is observed that for the normal macro strains the maximum micro stresses occur for normal components for both boundary layer and fully periodic problem. However, for the shear case both normal and shear micro strains can be the higher.

6.3.3. ***Variation of micro stresses along the depth of the RVE for 45° fibre orientation***

Finally, for the 45° fibre orientation the micro stress variations have been studied for different macro strains. The minimum and maximum values of micro stresses and their types, for boundary layer and fully periodic problems are reported in Table 14 and Table 15 for macro normal strain and shear strain cases, respectively. Further, the corresponding distribution of these micro stresses are shown in Fig. 21 for both normal and shear macro strains. From Table 14 it can be noticed that the maximum stress value occurs for $\sigma_{xx}^{(bl)}$ for all the three normal macro strains $\varepsilon_{(0),jj}$ for the boundary layer case. However, for the fully periodic case maximum stress value occurs for $\sigma_{(1),jj}$ corresponding to applied macro strain $\varepsilon_{(0),jj}$. Interestingly, it can be noticed that there is not much difference in stress values between the boundary layer and fully periodic problems for this particular fibre orientation contrary to the observations made earlier.

The stress value is maximum for the $\sigma_{yy}^{(bl)}$ for unit macro strain $\varepsilon_{(0),yz}$ which is 6.10*E*04 but for the fully periodic case it is only 7450. Interestingly, for $\varepsilon_{(0),xy}$ the maximum stress value for boundary layer and fully periodic problem are very close which is 1.33*E*04 and 1.38*E*04, respectively but for different micro stresses, i.e. $\sigma_{zz}^{(bl)}$ and $\sigma_{(1),xy}$.

6.4. *Variation of σ_{RMS} along the depth of different RVEs for boundary layer and fully periodic problem*

After studying the variation of micro strains and micro stresses for the RVEs with different fibre orientations, we have extended the study to the variation of RMS value of the micro stress, σ_{RMS} due to unit macro strains on these two scenarios. In this study, initially effect of macro normal strain is considered. Table 16 presents the σ_{RMS} values for the applied normal macro strain for both boundary layer and fully periodic problems. These values are reported for all the three RVEs. From this table, it can be noticed that in general, for the boundary layer the σ_{RMS} values are much higher compared to the fully periodic condition for all the three macro normal strains.

The σ_{RMS} values for macro shear strain cases for the three RVEs of boundary layer and fully periodic problems are reported in Table 17. From this table it is clearly seen that σ_{RMS} values are significantly higher for boundary layer problem than fully periodic problem for all the cases. Further, in case of boundary layer problem σ_{RMS} values for 45° RVE are significantly higher compared to those 0° and 90° RVEs for $\varepsilon_{(0),yz}$ and $\varepsilon_{(0),xz}$ cases whereas for $\varepsilon_{(0),xy}$ case it is higher in 0° RVE. Similarly, for fully periodic problem the maximum σ_{RMS} values are seen for $\varepsilon_{(0),yz}$, $\varepsilon_{(0),xz}$ and $\varepsilon_{(0),xy}$ cases in 90°, 0° and 45° RVEs, respectively.

Further, contour plots for the variation of σ_{RMS} are provided on the planes as shown in Fig. 15 from Fig. 22 to Fig. 25 for both fully periodic and boundary layer problems. Illustrative contour plots are shown only for macro strain $\varepsilon_{(0),zz}$ and $\varepsilon_{(0),yz}$ for both fully periodic (FP) and boundary layer (BL) problems. These plots also show the areas of high stress concentration. Damage initiation is expected to take place in these regions due to applied macro strains for different fibre orientation (for example, see Fig. 23).

It can be seen that σ_{RMS} values for boundary layer corrected solutions are significantly higher than those for fully periodic problem. It is also seen that σ_{RMS} values are more for applied macro shear strain cases than applied macro normal strain cases for all RVEs. Furthermore, these distributions show clear symmetry in case of applied macro normal strains. From Fig. 24 - Fig. 25, it is seen that the effect of shear loading is significant on σ_{RMS} for boundary layer problem.

Finally, we extended our study for the variation of maximum σ_{RMS} around the fibre-matrix interface. The variation is calculated for both boundary layer and fully periodic problem for 0° and 90° fibre orientation. Table 18 and Table 19 show the variation of maximum σ_{RMS} for boundary layer and fully periodic problem for 0° and 90° fibre orientations, respectively. The data is extracted around the fibre-matrix interface as shown in Fig. 26.

It is observed that for the RVE with 0° fibre orientation, the ratio is less that 1 for normal macro strain cases. However, for shear macro strain case, $\varepsilon_{(0),yz}$ the ratio is very high (see Table 18). However, for RVE with 90° fibre orientation, the ratio is high for normal macro strain case, $\varepsilon_{(0),yy}$ and shear macro strain cases, $\varepsilon_{(0),yz}$ and $\varepsilon_{(0),xz}$. Ratios for the other macro strain values are less than 1 (See Table 19). So, the ratio varies not only with the fibre orientation but also with the applied macro strain.

7. Conclusion

In this study, a novel approach to study the effect of boundary layer at the edge of the composite material is presented. The classical mathematical homogenization theory is modified from the interior of the domain to the edge of the composite material. The method presented uses the macro and fully periodic micro solution to determine a boundary layer correction term, which accounts for the mismatch in the

boundary displacement induced due to the fully periodic micro solution. The mismatch of the displacement drives the boundary problem corresponding to the boundary layer correction. This method gives a more accurate representation of the local stresses in the neighbourhood of the boundary. The method developed is used to study plies with three different fibre orientations. For the applied unit macro strains, variation of the micro strains and micro stresses are studied along strips terminating at the boundary. Variation of σ_{RMS} is studied in order to determine critical regions in the vicinity of boundary, which will be regions of damage initiation. Comparison with the classical two-scale solution shows a significant change in the local stress concentrations as a result of the boundary layer correction.

The major conclusions that can be drawn from this study are:

1. The boundary layer tail decays within 5–6 layers from the fixed edge.
2. The displacement norm shows exponential decay for the boundary layer problem. This is the classical St. Venant principle. Note that the rate of decay varies with the load type and fibre orientation.
3. The boundary correction leads to significant changes in the local strains, in the layer close to the boundary. Consequently, the variation of micro stresses is also similar. Interestingly, σ_{yz} and σ_{xz} increase significantly near the boundary, for almost all load cases and orientations considered. The increase can be as high as 772% for RVE with 90° fibre orientation.
4. The minimum and maximum values of micro strains and stresses for all the cases in this study vary from one RVE to another as it is noticed from the contour plots. This variation is mainly due to the orientation of the fibre. So, orientation of the fibre has a significant effect on the boundary layer tail to decay.
5. It is noteworthy that σ_{RMS} changes significantly when the boundary layer correction is added. The increase can be as high as 133% for $\varepsilon_{(0),xx}$ case of RVE with 0° fibre orientation. This is important as it completely changes the failure initiation mechanism (matrix normal or shear mode), failure load value and failure zones, in the vicinity of the boundary.

The method presented in this study can be easily extended to Neumann or Robin boundary conditions, leading to a better understanding of the mechanics near boundaries.

Appendix A. Supplementary data

Supplementary data to this article can be found online at https://doi.org/10.1016/j.compositesb.2019.05.026.

References

[1] Willis JR. The overall elastic response of composite materials. J Appl Mech 1983;50(4b):1202–9.
[2] Nemat-Nasser S, Hori M. Micromechanics: overall properties of heterogeneous materials, vol. 37. Elsevier; 2013.
[3] Aboudi J, Arnold SM, Bednarcyk BA. Micromechanics of composite materials: a generalized multiscale Analysis approach. Butterworth-Heinemann; 2012.
[4] Herakovich CT. Mechanics of composites: a historical review. Mech Res Commun 2012;41:1–20.
[5] Christensen RM. Mechanics of composite materials. Courier Corporation; 2012.
[6] Hill R. A self-consistent mechanics of composite materials. J Mech Phys Solids 1965;13(4):213–22.
[7] Christensen R, Lo KH. Solutions for effective shear properties in three phase sphere and cylinder models. J Mech Phys Solids 1979;27:315–30.
[8] Bakhvalov NS, Panasenko G. Homogenisation: averaging processes in periodic media: mathematical problems in the mechanics of composite materials, vol. 36. Springer Science & Business Media; 2012.
[9] Bensoussan A, Lions JL, Papanicolaou G. Asymptotic analysis for periodic structures, vol. 374. American Mathematical Soc.; 2011.
[10] Sanchez-Palencia E. Boundary layers and edge effects in composites. In: Homogenization techniques for composite media. Springer; 1987. p. 121–92.
[11] Suquet PM. Elastic perfectly plastic constituents. In: Homogenization techniques for composite media. Springer; 1987. p. 245–78.
[12] Sanchez-Palencia E. Homogenization in mechanics: a survey of solved and open problems. Rend. Sem. Mat. Univ. Politec. Torino 1986;44(1):1–45.
[13] Hollister SJ, Kikuchi N. A comparison of homogenization and standard mechanics analyses for periodic porous composites. Comput Mech 1992;10(2):73–95.
[14] Sanchez-Palencia E. Homogenization method for the study of composite media. In: Asymptotic analysis II. Springer; 1983. p. 192–214.
[15] Chen Q, Chen X, Yang Z, Zhai Z, Gao J. Micromechanical modeling of plain woven polymer composites via 3d finite-volume homogenization. Polym Compos 2018;39(9):3022–32.
[16] Tessitore N, Riccio A. A novel fem model for biaxial non-crimp fabric composite materials under tension. Comput Struct 2006;84(19–20):1200–7.
[17] Kuo CM. Elastic bending behavior of solid orthogonal woven 3-d carbon–carbon composite beams. Compos Sci Technol 2008;68(3–4):666–72.
[18] Byun JH, Whitney TJ, Du G-W, Chou T-W. Analytical characterization of two-step braided composites. J Compos Mater 1991;25(12):1599–618.
[19] Daudeville L, Ladevéze P. A damage mechanics tool for laminate delamination. Compos Struct 1993;25(1–4):547–55.
[20] Daudeville L, Allix O, Ladevéze P. Delamination analysis by damage mechanics: some applications. Compos Eng 1995;5(1):17–24.
[21] Baranger E, Allix O, Blanchard L. A computational strategy for the analysis of damage in composite pipes. Compos Sci Technol 2009;69(1):88–92.
[22] Kozlov S. Averaging differential operators with almost periodic, rapidly oscillating coefficients. Sb Math 1979;35(4):481–98.
[23] Babuška I. Homogenization and its application. mathematical and computational problems. In: Numerical solution of partial differential equations–III. Elsevier; 1976. p. 89–116.
[24] Panasenko GP. Asymptotics of higher orders of solutions of problems on the contact of periodic structures. Matem. sb. 1979;110(152):505–38.
[25] Panasenko GP. Higher order asymptotics of solutions of problems on the contact of periodic structures. Sb Math 1981;38(4):465–94.
[26] Panasenko GP. Multi-scale modelling for structures and composites, vol. 615. Springer; 2005.
[27] Allaire G, Amar M. Boundary layer tails in periodic homogenization. ESAIM Control, Optim Calc Var 1999;4:209–43.
[28] Tartar L. The general theory of homogenization: a personalized introduction, vol. 7. Springer Science & Business Media; 2009.
[29] Dumontet H. Study of a boundary layer problem in elastic composite materials. ESAIM Math Model Numer Anal 1986;20(2):265–86.
[30] Fish J, Yu Q. Multiscale damage modelling for composite materials: theory and computational framework. Int J Numer Methods Eng 2001;52(1–2):161–91.
[31] Galvanetto U, Aliabadi M. Multiscale modeling in solid mechanics: computational approaches, vol. 3. World Scientific; 2010.
[32] Santosa F, Vogelius M. First-order corrections to the homogenized eigenvalues of a periodic composite medium. SIAM J Appl Math 1993;53(6):1636–68.
[33] Gérard-Varet D, Masmoudi N. Homogenization and boundary layers. Acta Math 2012;209(1):133–78.
[34] Andrianov IV, Danishevskyy VV, Weichert D. Boundary layers in fibrous composite materials. Acta Mech 2011;216(1–4):3–15.
[35] Soden P, Hinton M, Kaddour A. Lamina properties, lay-up configurations and loading conditions for a range of fibre-reinforced composite laminates. Compos Sci Technol 1998;58(7):1011–22.